Karlsruher Institut für Technologie

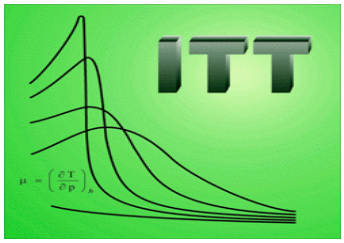

Modelling and Numerical Simulation of Turbulent Reactive Flows (Modellierung und numerische Simulation turbulenter reaktiver Strömungen)

Bachelor thesis of

Lovish Chopra

Institute of Technical Thermodynamics (ITT)

Karlsruhe Institute of Technology, Germany

Supervisor**: Dr. Ing Chunkan Yu**

15th March 2021- 15th July 2021

Statement by the author

I here declare that I have written this thesis independently. It contains no unfair or unauthorized resources Every single content which was taken directly or indirectly from other sources, it has been indicated through the fair means and the sources are referenced according to the official ways.

This bachelor thesis is identical with the assessed thesis that has been submitted in the electronic form.

Karlsruhe, July 2021 ……...

Lovish Chopra Signature

Acknowledgement

The completion of any inter-disciplinary research project/thesis depends upon the cooperation, determination and the combined efforts of several sources of knowledge and along with all the mentors. It would not have been possible for me to accomplish this task without the guidance and proper motivation from my supervisors, professors, friends and support from my family.

I am very grateful to my supervisor/mentor *Dr. Ing Chunkan Yu, Institute of Technical thermodynamics, Department of Mechanical Engineering, Karlsruhe Institute of Technology, Germany* for his valuable advice and guidance through each step of the way. I am thankful to him for providing me with direction and motivation for the thesis.

I would also like to acknowledge *Prof. Dr. rer. nat. habil. Ulrich Maas for* providing me this opportunity in his research institute and with his permission I can contribute to this topic.

I also owe my deepest gratitude to my friends in India and Germany for their help and guidance in possibly reading and making amendments in my thesis.

Last but not the least, I would like to thank my family for the continuous support for everything that I have achieved in my career, this being the most prestigious to me till this moment.

Abstract

Turbulent Combustion poses a lot of challenges in various aspects of engineering. Since Direct Numerical Simulations (DNS) take an unbearable computational effort to accurately predict the nature of these flames by resolving to the lowest possible turbulent scales without modelling, these processes need to be modelled using appropriate methods for better understanding. Non-premixed turbulent combustion is of great interest to research in the field related to modelling of particle treatment in a particular defined method. For this purpose, the statistical approach to turbulent reactive flows is adopted by the help of Probability Density Functions (PDF). In this same regard as the use of detailed reaction mechanisms take a lot of computational power in the aim to take Turbulence-Chemistry Interactions into account, reduced description of the kinetics with appropriate number of species in considered with the help of methods based on Reaction-Diffusion Manifolds (REDIM). This work is mainly concentrated towards two different Particle Mixing Models – Modified Curl's Model (MCM) and Velocity Conditioned Multiple Mapping Closures (MMC) which are coupled with the above methods to simulate piloted non-premixed methane flames (Sandia Flame D) and validated with the experimental data.

Secondly, partially premixed turbulent flame using inhomogeneous inlets is modelled using RANS and Finite Rate Chemistry, as LES for partially premixed turbulent flame still remains an open challenge despite its greatness. Sydney Burner is simulated in Ansys Fluent in order to gain insight on behavior of different species and temperature at different axial locations for a particular configuration and operating condition. Results are validated with Experimental Temperature Measurements from Sydney University taken with the help of line-imaged Raman/Rayleigh scattering and Laser induced Fluorescence (LIF) of CO.

Zusammenfassung

Turbulente Verbrennung stellt viele Herausforderungen in verschiedenen Aspekten der Technik. Da direkte numerische Simulationen (DNS) einen unerträglichen Rechenaufwand erfordern, um die Natur dieser Flammen durch Auflösung in die niedrigstmöglichen turbulenten Skalen ohne Modellierung genau vorherzusagen, müssen diese Prozesse zum besseren Verständnis mit geeigneten Methoden modelliert werden. Die turbulente Verbrennung ohne Vormischung ist von großem Interesse für die Forschung auf dem Gebiet der Modellierung der Partikelbehandlung in einem bestimmten definierten Verfahren. Dazu wird der statistische Ansatz für turbulente reaktive Strömungen mit Hilfe von Probability Density Functions (PDF) übernommen. Ebenso wie die Verwendung detaillierter Reaktionsmechanismen viel Rechenleistung erfordert, um Turbulenz-Chemie-Wechselwirkungen zu berücksichtigen, wird eine reduzierte Beschreibung der Kinetik bei entsprechender Anzahl der betrachteten Spezies mit Hilfe von Methoden basierend auf Reaktions- Diffusionsverteiler (REDIM). Diese Arbeit konzentriert sich hauptsächlich auf zwei verschiedene Partikelmischmodelle – Modified Curl's Model (MCM) und Velocity Conditioned Multiple Mapping Closures (MMC), die mit den oben genannten Methoden gekoppelt sind, um pilotierte nicht vorgemischte Methanflammen (Sandia Flame D) zu simulieren und validiert mit die experimentellen Daten.

Zweitens wird eine teilweise vorgemischte turbulente Flamme mit inhomogenen Einlässen mit RANS und Finite-Rate-Chemie modelliert, da LES für teilweise vorgemischte turbulente Flammen trotz ihrer Größe immer noch eine offene Herausforderung bleibt. Sydney Burner wird in Ansys Fluent simuliert, um Einblicke in das Verhalten verschiedener Spezies und Temperaturen an verschiedenen axialen Positionen für eine bestimmte Konfiguration und Betriebsbedingung zu erhalten. Die Ergebnisse werden mit experimentellen Temperaturmessungen der Sydney University validiert, die mit Hilfe von linienbildender Raman/Rayleigh-Streuung und laserinduzierter Fluoreszenz (LIF) von CO aufgenommen wurden.

Table of Contents

1. Introduction

Combustion has become a necessity in almost every aspect of industrial engineering especially in domains of mechanical and aerospace engineering [1-3]. Today, simulations have taken methodology of design of a particular model to a whole new level. Especially for the processes that have been quite difficult to conduct physically or experimentally, simulations have helped in progress to a great extent.

As of this consequence, different challenges are posed towards development of various methods and modelling techniques in order to tackle this area, especially in turbulent combustion [3-7]. Combustion consists of dealing with both aspects of Fluid Mechanics as well as Chemical Kinetics [1,3,5]. Quantities like velocity, turbulent kinetic energy etc. need to determined well to describe phenomenon of turbulent Flows. Moreover, taking care of fluid mechanics doesn't fully solve the purpose as Chemical Kinetics further pose complex problems. Chemical Kinetics is concerned towards determining of rate of formation of products and consumption rate of reactants. Both of these phenomena are themselves in complex that simulations of turbulent Reactive Flows which couples both fluid mechanics and chemical kinetics, raises the level of complexity by a significant level as modelling required to study turbulence-chemistry interactions poses a major challenge.

Though there are different turbulent scales eg: - as those in DNS and LES [7] that can be considered while solving a problem, RANS [3,5,7] gives quite a good advantage in terms of computational cost and grid requirements giving the reason to use its methodology in this thesis. Besides this, use of Probability Density Functions (PDFs) [16] is adopted in this work which takes the statistical nature of turbulent flows. It enables to express the variables in thermo-kinetic space within their event of occurrence in their respective sample space. Transported PDF equation is derived from Navier-Stokes after in which conditional diffusion terms needs to be modelled. In the aim to achieve that, various mixing models are proposed in the past [20-23]. However, each one or the other has a limitation that can't be neglected. In this thesis, major focus is towards the molecular mixing models and as that of which Modified Curl's Model (MCM) and newly proposed methodology for Velocity Conditioned Multiple

Mapping Closure Model (VC-MMC) are tested for turbulent non-premixed methane piloted flames, Sandia Flame Series D.

Secondly, research in partially premixed form of combustion has also quite progressed in the past few years [50-55]. So as to get insights of the same, Sydney partially premixed methane piloted flame is simulated in Ansys Fluent with Finite Rate chemistry under a particular burner configuration.

This thesis commences with some introduction to basics of combustion in chapter 2 which summarizes the general concepts, governing equations and different types of flames. Further, the concept of turbulent reactive flows is explained in chapter 3. Then in Chapter 4, approach to turbulent reactive flows using probability density functions is explained how it is used to deal with scalars. Chapter 5 highlights the concept for MCM and approach for VC-MMC Model along with their algorithms used in this thesis. Afterwards, the methodology used in turbulent non-premixed piloted flames is described in chapter 6 along with the solution and numerical procedure used to model these flames i.e. by the PDF particle approach. Further in chapter 7, methodology for modeling Partially premixed flames is explained followed by the proper solution procedure followed for its treatment. Finally, results and observations are discussed in chapter 8 as drawn from the two methodologies proposed in each of the respective chapters and a final conclusion is stated in chapter 9 after reviewing all the results.

2. Basics of Combustion

2.1 General Theory

The explanation of basic and phenomenon combustion processes can be very well described with the help of basic definitions and fundamental concepts at the molecular and global frames of reference in regard to which [1] they have been described in brief below.

1. *Heat of Reaction*

   The Heat of Reaction (also known and Enthalpy of Reaction) is the change in the enthalpy of a chemical reaction that occurs at a constant pressure. It is a thermodynamic unit of measurement useful for calculating the amount of energy per mole either released or produced in a reaction. Since enthalpy is derived from pressure, volume, and internal energy, all of which are state functions, enthalpy is also a state function.

2. *Standard Heat of Reaction*

   It is defined as the heat of reaction at some standard pressure and temperature as required to describe a combustion application or process.

   For example: - say at 1 bar, 298 K, $\Delta H_{f_o} \rightarrow 300\ KJ/mole$.

3. *Heat of Formation*

   Heat of Formation defined for a particular pressure and temperature is the negative heat of reaction at those state values for a component formed from its 'reference elements'. Reference Elements can specifically be categorized as $C(s), H_2, N_2, O_2$ etc.

$$H_2 + \frac{1}{2}O_2 \rightarrow H_2O$$

$$C(s) + O_2 \rightarrow CO_2$$

The above two reactions (1) and (2) can be perfectly described as the formation reactions for $H_2O\ and\ CO_2$ respectively.

Formation of one species from its own element(s) can also be described as the formation reactions. For example,

$$\frac{1}{2}O_2 \rightarrow O$$
$$O_2 \rightarrow O_2$$

4. *Sensible Enthalpy*

Sensible Enthalpy basically describes how good a fuel is. Let's consider a general example of heat of reaction through the following equation.

$$\Delta H = H_2 - H_1 = \sum_{i=1}^{N} n_i'' \Delta h_{f_{m_i}}(P_2, T_2) - \sum_{i=1}^{N} n_i' \Delta h_{f_{m_i,}}(P_1, T_1)$$

Where, $n_i''$is number of moles of species 'i' in the products, n_i' number of moles of species 'i' in the reactants. Subscripts describe the states before and after the chemical reaction respectively.

$$h_{f_{m_i}}(T) = \Delta H_f^o{}_{298} + \left(h_{f_{m_i}}(T) - h_f^o{}_{298_{mi}} \right)$$

Again, $h_{f_{m_i}}(T)$ is specific molar enthalpy, $\Delta H_f^o{}_{298}$ as the standard heat of formation and $(h_{f_{m_i}}(T) - h_f^o{}_{298_{mi}})$ is the Sensible Enthalpy.

Sensible Enthalpy can be expressed as: -

$$h_{f_{m_i}}(T) - h_f^o{}_{298_{mi}} = \int_{T_{ref}}^{T} C_{p_{m_i}}(T)dt$$

For calorifically perfect gas, sensible Enthalpy = $C_{p_{m_i}}\left(T - T_{ref}\right)$, where T_{ref} is preferred as 298.15 K.

Since the process is adiabatic, hence we'll have $H_2 = H_1$. Now comparing the LHS and RHS after expanding the equation for ΔH.

$$\sum_{i=1}^{N} n''_i \left\{ \Delta H_f^o{}_{T_{ref}} + \mathrm{h_f^o}(T_{adiabatic}) - h_f^o\left(T_{ref}\right) \right\}_{M_i}$$
$$= \sum_{i=1}^{N} n'_i \left\{ \Delta H_f^o{}_{T_{ref}} + \mathrm{h_f^o}(T_1) - h_f^o\left(T_{ref}\right) \right\}_{M_i}$$

The above equation simply means that the sensible enthalpy of the products will be high, consequence of which the heat of formation needs to be low (as the RHS is fixed). Mixture composition significantly has an enormous effect on heat of formation for stable products. For example, stoichiometric mixtures (which will be explained later in this chapter) have the highest negative heats of formations which ultimately leads to the highest Adiabatic Flame Temperature ($T_{adiabatic}$).

5. *Chemical Kinetics*

Chemical Kinetics, also known as the reaction kinetics is the branch of physical chemistry dealing with the concepts and understanding of the rates of the chemical reactions. Chemical Kinetic modelling is an important aspect in describing a basic combustion phenomenon. These are coupled with fluid mechanics models in the aim to understand the practical combustion ideas [2].

a) Mass concentration of species $i = \rho_i$ (density) = $\frac{mass\ of\ species\ i}{Volume\ of\ the\ mixture}$

b) Molar concentration of species $i = C_i = \frac{number\ of\ moles\ of\ species\ i}{Volume\ of the\ mixture}$

Density of the mixture = $\sum_{i=1}^{N} \rho_i$

Concentration of the mixture = $\sum_{i=1}^{N} c_i$

6. *Mass Transfer Concepts*

a) Mass Averaged Velocity of a mixture

It is defined as the average velocity of the mixture with which it is progressing independent of what other species are doing in the whole mixture.

$$\vec{v} = \left(\frac{\sum_{i=1}^{N} \rho_i \overrightarrow{v_i}}{\sum_{i=1}^{N} \rho_i}\right.$$

b) Molar Averaged Velocity of the mixture

It can be stated as in the similar context with mass averaged velocity but molar concentration of species is considered instead of density of individual species.

$$\overrightarrow{v^*}=(\frac{\sum_{i=1}^{N} c_i\overrightarrow{v_i)}}{\sum_{i=1}^{N} c_i}$$

c) Mass diffusion Velocity of species $i = \vec{V} = \overrightarrow{v_i} - \vec{v}$

d) Molar diffusion Velocity of species $i = \overrightarrow{V^*} = \overrightarrow{v_i} - \overrightarrow{v^*}$

$\overrightarrow{V}$ and $\overrightarrow{V^*}$ represent what species are doing instead of going along with the flow.

e) Mass and molar flux of species i can be stated as $\overrightarrow{m_i} = \rho_i\overrightarrow{v_i}$ and $\overrightarrow{n_i} = c_i\overrightarrow{v_i}$.

f) Relative Mass and molar diffusion flux for particular species i can be written as $\overrightarrow{J_i} = \rho_i(\overrightarrow{v_i} - \vec{v})$ and $\overrightarrow{J^*} = c_i(\overrightarrow{v_i} - \overrightarrow{v^*})$.

7. Equivalence Ratio (ϕ)

It is defined as the ratio of actual fuel to air ratio in a mixture to stoichiometric fuel to air mixture.

If $\phi = 1$, stoichiometric condition i.e., if fuel and oxidizer consume each other completely.

$\phi < 1$ signifies the fuel lean condition (oxidizer rich).

$\phi > 1$ signifies the fuel rich condition (oxidizer lean).

2.2 Governing Equations

Combustion Processes involve a vast space of transport equations i.e., convection, diffusion and Chemical Reactions [3,4,1] and they are solved using different discretization schemes in space and time. All the equations thereby will be presented in their respective differential forms. Different terms describe different aspects of problem required to model.

Continuity Equation

$$\frac{\partial \rho}{\partial t} + \nabla.(\rho V) = 0$$

Momentum Conservation Equation

$$\frac{\partial Y_i}{\partial t} + v.\nabla v = -\nabla.q/\rho + \rho \sum_{i=1}^{N} Y_i f_i$$

Species Mass Conservation Equation

$$\frac{\partial Y_i}{\partial t} + v.\nabla Y_i = \frac{w_i}{\rho} - \frac{[\nabla.(\rho Y_i V_i)]}{\rho_i} \qquad i = 1,2,\ldots.N$$

Energy Conservation Equation

$$\rho \frac{\partial u}{\partial t} + \rho v.\nabla v = -\nabla.q - P:(\nabla v) + \rho \sum_{i=1}^{N} Y_i f_i.V_i \qquad i = 1,2,\ldots.N$$

Ideal Gas Equation

$$p = \rho R^o T \sum_{i=1}^{N} (Y_i/W_i)$$

2.3 Different division of Flames

In combustion, the nature of flames mainly depends on whether the fuel and oxidizer are mixed before burning (premixed) or after burning (non-premixed) [3]. When the flow is also laminar alongside burning of these flames, they are often categorized into Laminar premixed and Laminar Non-premixed Flames. Similarly, if the flow becomes turbulent, they can be termed as Turbulent Premixed or Non-premixed Flames. A special combustion case popularly known as partially premixed is the one in which unburnt mixture is not completely or fully mixed before entering the combustion zone. The following illustration from [5] presents the applications for all these flames along with their occurrences in different engineering fields and applications.

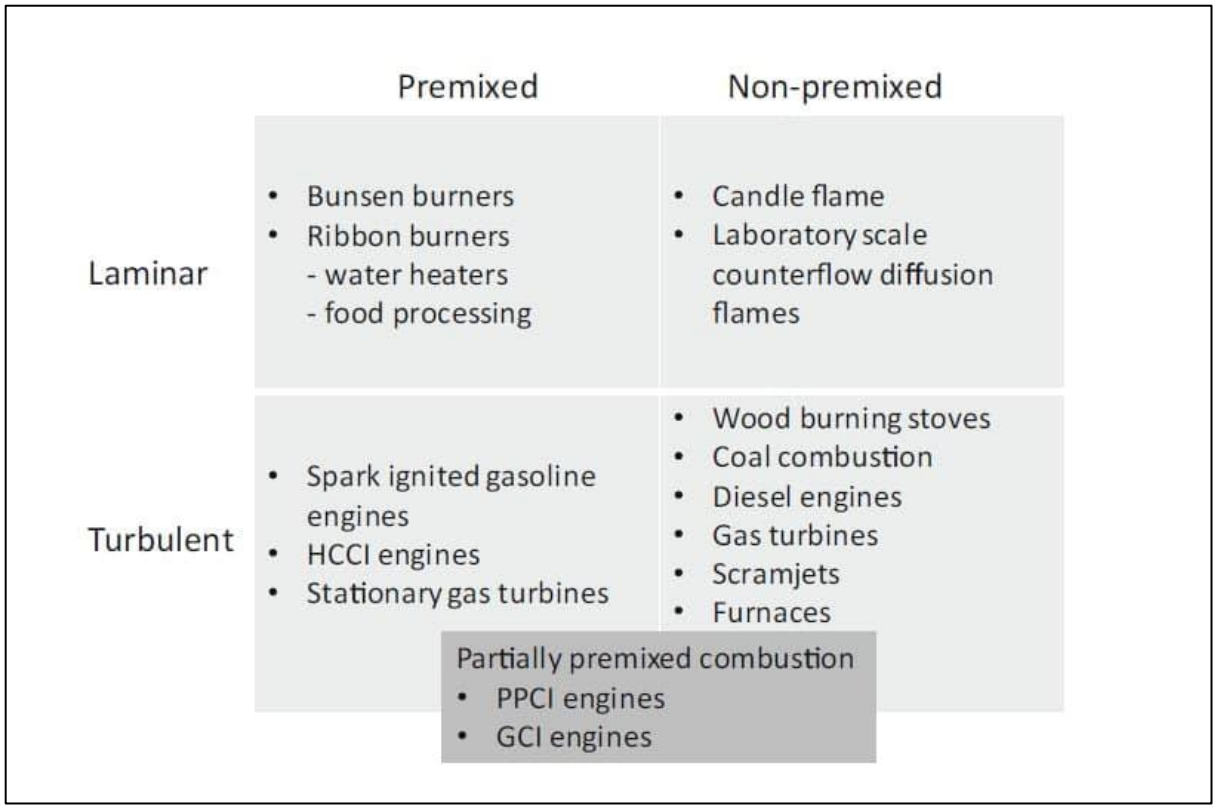

Figure 1: Different Applications for different flames [5]

3. Turbulent Reacting Flows

3.1 Conceptual Description

The Most important non-dimensional quantity describing the nature of the flow and its tendency to exhibit a turbulent regime from a lamina is the Reynolds Number, which is often described as the Ratio of Inertial forces to viscous forces [6].

$$Re = \frac{\rho u L}{\mu}$$

Where ρ is the flow density, u is the flow velocity, L is the characteristic length (diameter in case of circular pipes) and μ is the dynamic viscosity. If the Reynolds number of a flow is low beyond a certain limit, flow is stable and stays laminar. However, in case of a turbulent flow where Reynolds number is predominantly high, it generally leads to the description of turbulent flow [7]. Moreover, turbulence of a flow is also promoted because of the energy cascade phenomenon in governing turbulence. The large eddy breaks up process is further transferred to small eddies in the process of energy transfer from former ones to latter, thus leading to dissipation of Kinetic Energy [7]. The efficiency of resolving the turbulence significantly depends on the length scales taken into consideration which will be described briefly in next section (3.1.1).

3.2 Length Scales in turbulent Flames

Turbulent Length Scales (length scales related to turbulence only)

The concept of Energy Cascade as discussed [7], gives a quite well description about dissipation of kinetic energy w.r.t the inertial subrange. The size of the eddies varies widely in a turbulent flow from largest eddies of length scale (l_o) or integral length scale upto smallest length scale (l_k) (kolmogorov length scale) [7,8]. Therefore, taking the proper length scale into consideration for a characteristic velocity u' , reynolds number for a turbulent flow can be related as follows [7],

$$Re_{l_o} = \frac{\rho u' l_o}{\mu}$$

$$Re_{l_k} = \frac{\rho u' l_k}{\mu}$$

Where, Re_{l_o} and Re_{l_k} is the turbulent Reynolds number and Kolmogorov Reynolds number. The ratio of smallest to largest length scales can be approximated [7] as: -

$$\frac{l_k}{l_o} \sim Re_{l_o}^{-\frac{3}{4}}$$

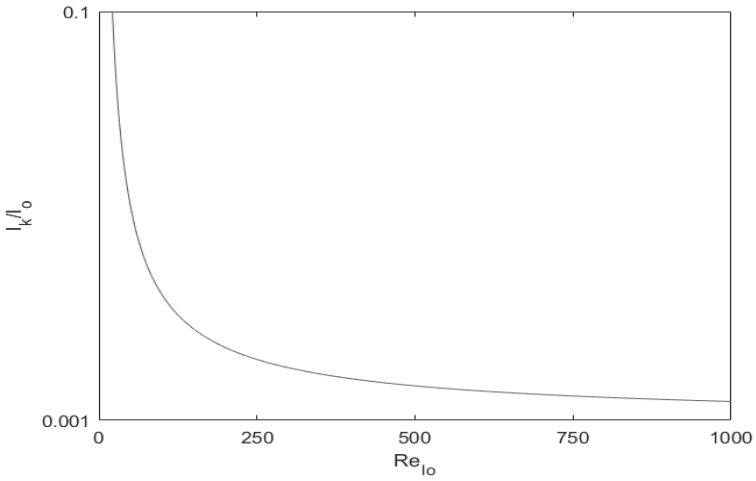

Figure 2: Variation of length scales w.r.t Turbulent Reynolds Number

CFD simulations which involve direct modelling with resolving eddies to smallest possible scale (Kolmogorov scales) are termed as *Direct Numerical Simulations* [7]. However, the computational cost for a DNS over other available turbulence models still tends to be a challenge [9,10]. Dependency over grid points for a 3-Dimensional DNS is presented by the following relation.

$$N_{Total} = Re^{\frac{9}{4}}$$

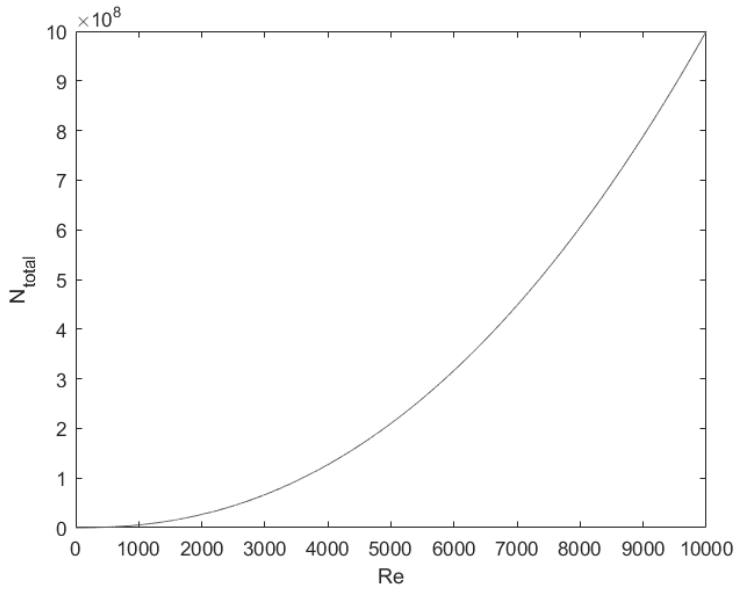

Figure 3: Grid size requirements for increasing Reynolds Number

Flame related Length Scales

In turbulent flames, especially non-premixed flames, not only turbulent length scales related to turbulence need to be resolved, but length scales related to flame size and structure must also be resolved [1,8,3], which further increase the computing demand for these simulations and make them more complicated.

Different length scales are defined especially in terms of thickness in context of flame configuration are described below briefly.

- δ_d – Diffusion thickness: - This is the layer for diffusion process that fuel and oxidizer diffuse towards each other and mix with each other according to the requirements [1,8]. Grid size should at least be this much refined in order to capture these diffusion processes and can be appropriately resolved.
- δ_r – Reaction thickness -: This are the regions in the computational domain where the reaction between different species takes place. They are usually smaller than quite a large factor than diffusion thickness [1,3]. Another condition on modelling of the computational domain is imposed i.e., the cell or the grid size must be small enough so that reaction zone can be well determined.

  Generally, $\delta_d \sim l_k \gg \delta_r$

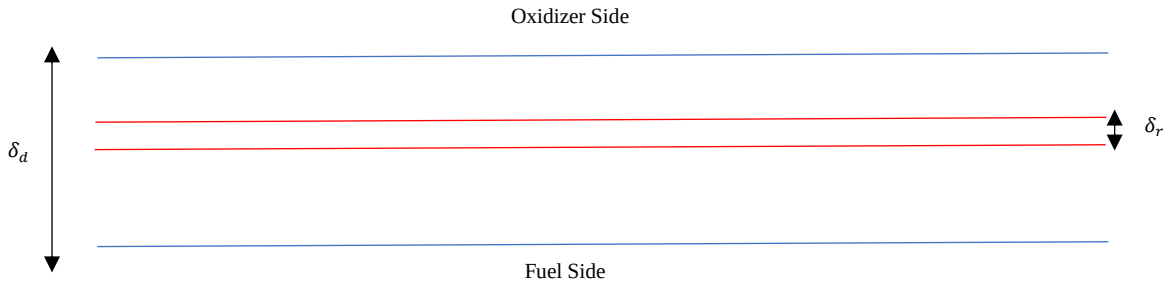

Figure 4: Different Length Scales in Turbulent non-premixed flames

Since the above requirements definitely require a significant increase in the number of cells required to model the computational domain than those described in the previous section the overall cost of a Direct Numerical Simulation is tremendously increased [11].

To conclude, due to heavy computational cost it's not wise to apply DNS approach to various engineering Applications. To overcome this issue, Reynolds Averaged Navier Stokes (RANS) model has been quite successful despite having some issues to capture detailed turbulent descriptions [3,5,7]. Large Eddy Simulations (LES) approach is quite popular as it is the mid-way between RANS and DNS [7] despite having some limitations [7].

3.3 RANS Model

3.3.1 Fundamental

In Reynolds Averaged Navier Stokes (RANS), all the governing equations are solved for the averaged quantities [7]. RANS simulations as compared to DNS and LES, has noticeable advantages in terms of computational requirements and geometry considerations [7] as of which it is quite well adopted in engineering and industrial applications [12]. Further ahead in the section, highlighted topics will include the major discussions for this model and its limitations and its measures.

Time Averaging and Favre Averaging

All the major quantities in the turbulent flows are characterized over steadiness and art of variation with time. If these quantities are not sufficiently damped (means having a large variation over time), time or Favre averaging has to be done depending upon the nature of flow.

Averaged Quantity is defined by taking average over a certain time interval over time given by a specific range $\Delta t = t_2 - t_1$.

$$\overline{f(x)} = \frac{1}{\Delta t}\int_{t_1}^{t_2} f(x,t)dt$$

where $f(x,t)$ is a random turbulence quantity (velocity, temperature or species mass fraction) at any random location. Once the above instantaneous quantity $f(x,t)$ is obtained, it can be split into its average value $\overline{f(x,t)}$ and fluctuating value $f'(x,t)$ for the same defined physical properties as,

$$f(x,t) = \bar{f}(x) + f'(x,t)$$

For most turbulent combustion problems as illustrated [5], Favre averaging is proved to be more useful as compared to time averaging because of large variations in density [3,7]. Thus, a density weighted average, $\widetilde{f(x)}$, which is called Favre average.

$$\widetilde{f(x)} = \overline{\left(\frac{\rho . f(x,t)}{\bar{\rho}}\right)}$$

Similar to the equation for Reynold's average, Favre instantaneous quantity can be presented as Favre averaged quantity $\widetilde{f(x)}$ and favre fluctutation $\widetilde{f''(x,t)}$, given in the below equation as follows: -

$$f(x,t) = \widetilde{f(x)} + \widetilde{f''(x,t)}$$

3.3.2 Governing Equations

Based on Favre averaging (this being the most relevant in turbulent reactive flows [3]), following equations can be formulated [3,7].

Favre Averaged Mass Conservation Eqn

$$\frac{\partial \bar{\rho}}{\partial t} + \frac{\partial \bar{\rho}\widetilde{u_j}}{\partial t} = 0$$

Favre Averaged Momentum Conservation Eqn

$$\frac{\partial \bar{\rho}\widetilde{u_i}}{\partial t} + \frac{\partial}{\partial x_j}(\bar{\rho}\widetilde{u_i}\widetilde{u_j} + \bar{p}.\delta_{ij}) = \frac{\partial}{\partial x_j}(\bar{\tau}_{ij} - \bar{\rho}\widetilde{u''u_j''})$$

Favre Averaged Species Conservation Eqn

$$\frac{\partial(\bar{\rho}\widetilde{w_k})}{\partial \mathrm{t}} + \frac{\partial}{\partial x_j}\left(\bar{\rho}\widetilde{u_j}\widetilde{w_k}\right) = \frac{\partial}{\partial x_j}\left(\bar{\rho}D_k\left(\frac{\partial\widetilde{w_k}}{\partial x_j}\right) + \bar{\rho}\widetilde{\dot{w}}_k - \frac{\partial}{\partial x_j}\left(\bar{\rho}\widetilde{u_j''w_k''}\right)\right.$$

For statistically stationary turbulent flows, terms with derivatives w.r.t time do not change with time, so therefore,

$$\frac{\partial(\bar{\rho})}{\partial t} = 0$$

$$\frac{\partial(\bar{\rho}\tilde{u}_i)}{\partial t} = 0$$

$$\frac{\partial(\bar{\rho}\widetilde{w}_k)}{\partial t} = 0$$

Apparently, the averaged Reynolds stresses $\bar{\rho}\widetilde{u''u_j''}$ in the momentum conservation equation, $\widetilde{\dot{w}}$ in $\bar{\rho}\widetilde{u_j''w_k''}$ for species conservation need to modelled to close the set of equations and have equal equations for same number of unknowns [7]. This can also be defined as the closure problem in RANS modeling [7,13,14].

Overcoming Closure Problem

As discussed in the previous section, one needs to overcome the closure problem in RANS modeling to get appropriate results. A method described by Pope [7] is the most popular approach in the turbulent viscosity model to tackle this problem. The turbulent viscosity model is given by: -

$$\bar{\rho}\widetilde{u''u_j''} = -2\mu_T\left(\widetilde{S_{\iota J}} - \frac{1}{3}\left(\frac{\partial\widetilde{u_k}}{\partial x_k}\right)\right) + \frac{2}{3}\tilde{\rho}k\delta_{i\,j}$$

where μ_T is the turbulent viscosity, k is the specific turbulent kinetic energy and $\widetilde{S_{\iota J}}$ is the mean strain rate tensor are given by the following expressions.

$$k = \frac{1}{2}\widetilde{u_{\iota J}''u_{\iota J}''}$$

$$\widetilde{S_{\iota J}} = \frac{1}{2}\left(\frac{\partial\widetilde{u_\iota}}{\partial x_j} + \frac{\partial\widetilde{u_J}}{\partial x_i}\right)$$

One method described briefly below is to determine μ_T is using two equation standard $k-\epsilon$ turbulence model governing equations for k and ϵ thus making it quite easy to model Reynold stresses. Alternatively, one equation model [7] and $k-\omega$ model can also be used instead of proposed turbulence model.

The most widely used two equation model is the standard $k-\epsilon$ turbulence model [13-15]. The underlying assumption of this model is that the turbulent viscosity is isotropic, in other words, the ratio between Reynold stress and mean rate of deformations is the same in all directions. Governing equations can be derived for both the variables using properties of conservativeness, tranportiveness and boundedness [7] and are illustrated as follows: -

For turbulent Kinetic energy k,

$$\frac{\partial(\rho k)}{\partial t}+\frac{\partial(\rho k u_i)}{\partial x_i}=\frac{\partial}{\partial x_j}\left[\frac{\mu_t \partial k}{\sigma_k \partial x_j}\right]+2\mu_t E_{ij}E_{ij}-\rho\epsilon$$

For turbulent dissipation rate ϵ,

$$\frac{\partial(\rho\epsilon)}{\partial t}+\frac{\partial(\rho u_i \epsilon)}{\partial x_i}=\frac{\partial}{\partial x_j}\left[\frac{\mu_t \partial \epsilon}{\sigma_\epsilon \partial x_j}\right]+2\frac{C_{1\epsilon}\epsilon}{k}\mu_t E_{ij}E_{ij}-\frac{C_{2\epsilon}\rho\epsilon^2}{k}$$

where μ_i represent velocity component in corresponding direction, E_{ij} represents component of rate of deformation, μ_t represents eddy viscosity is related to k, ϵ, ρ and C_μ as follows: -

$$\mu_t=\frac{\rho C_\mu k^2}{\epsilon}$$

The above governing equations also consist of model constants $\sigma_k, \sigma_\epsilon, C_{1\epsilon}, C_{2\epsilon}$ and C_μ and default values are considered [7,16] until any further changes are required.

Modelling of Averaged Reaction Rate

The high non-linearity of the term averaged reaction rate $\widetilde{\omega}$ poses a major issue in the modelling of the essential equations [1,3]. This is cause from two main issues, first being the non-linearity due to species concentrations and second being its highly non-linear dependency on temperature.

4. Probability Density Functions

4.1 Introduction

The aim of using the probability density functions is to calculate the basic flow properties like velocity, temperature, enthalpy and species concentrations for treatment of turbulent reactive flows. The PDFs provide a statistical description of the state of fluid at each point in the flow field along with its statistical behavior [16].

Firstly, in section 4.2 along with its statistical concept, advantages and limitations of one-point PDFs will be described. Secondly, the concept of joint-pdfs will be explained in the section 4.3 closed finally with a modelled transport equation for the widely used velocity-composition joint pdf (for the three components of velocity and composition variables i.e., species mass fractions and enthalpy) [16]. Finally, the last section highlights the method of particle method in order to obtain solution of the transported PDF Equation. Main idea behind the particle approach is the modelling of particle velocity, frequency, molecular mixing (along with corresponding particle mixing models) which will be briefly described. Evolution of particle's thermo-kinetic state (vector for composition variables) will also be highlighted.

4.2 Statistical Definition

4.2.1 Random Variable Concept

The basic understanding of the random variables is required in the conceptual clearance of PDFs. To illustrate this, a mixing layer experiment is considered in which two consecutive values of the random variable ϕ is measured at a certain location x_o and time t_o[16] and are locally termed as $\phi'(x_o, t_o)$ and $\phi''(x_o, t_o)$. They can be thought of obeying the below relation:

$$\phi'(x_o, t_o) \neq \phi''(x_o, t_o)$$

Due to the nature of the turbulent flows, these two quantities have to be certainly different [7,16]. This is mainly because of the reason that initial and boundary conditions, though mathematically same, are not identical. Small perturbations before the start of the experiment due to first one lead to slight change in boundary conditions for the second. Governing equations for the flow, theoretically being the same, can change due to the changes in the fluid

or air properties. These differences, however small, can create a lot of differences in temperature and velocity fields [16].

One can conclude that in any turbulent flow experiment, the boundary and initial conditions can't be controlled for the nature of flow to be accurately determined [16]. Therefore, it gives the reason to treat the flow properties as a random variable. Temperature ($T(x_o, t_o)$), axial Velocity ($U(x_o, t_o)$), enthalpy ($h(x_o, t_o)$) etc... can be treated as the flow random variables [16].

4.2.2 One Point joint PDFs

Two random variables along with their consecutive sample space are considered in order to make things much easier to comprehend. Let $\phi(x_o, t_o)$ and $U(x_o, t_o)$ be the random variable for the normalized temperature and normalized axial velocity at a particular location x_o and time t_o, ψ and V being their sample spaces so that any value for a particular random variable (ϕ and U) can be plotted on them [16].

For random variable U with sample space V, distribution function and pdf can be written respectively as $F_u(V)$ and $f_u(V)$ [16] and can be defined as follows: -

$$F_u(V) \equiv P(U < V)$$

and,

$$f_u(V) = \frac{dF_u(V)}{dV}$$

These exact can definitions and properties can be constituted for ϕ as well. Mean and Variance can consecutively be defined as in [16]: -

$$\langle U \rangle = \int_{-\infty}^{\infty} V f_u(V) dV$$

$$\mathbf{D}(U) = \langle u^2 \rangle = \int_{-\infty}^{\infty} (V - \langle U \rangle)^2 f_u(V) dV$$

where u is the fluctuation i.e., the difference between normalized and averaged or mean component,

$$u \equiv U - \langle U \rangle$$

The distribution functions $F_{\phi}(\psi)$ and $F_{u}(V)$ provides all the information about their respective random variables separately but not any joint information [16]. The probabilities for their joint occurrences can't be properly known despite of having each one of them. This information is provided by the joint event $\phi < \psi$ and $U < V$ having its joint distribution function $F_{u\phi}(V, \psi)$ which is defined [16] as

$$F_{u\phi}(V, \psi) \equiv \mathbf{P}(U < V, \phi < \psi)$$

The following properties of the joint distribution function are prescribed as follows:

$$0 \leq F_{u\phi}(V, \psi) \leq 1,$$

$$F_{u\phi}(-\infty, \psi) = F_{u\phi}(V, -\infty) = 0,$$

$$F_{u\phi}(\infty, \psi) = F_{\phi}(\psi),$$

$$F_{u\phi}(V, \infty) = F_{u}(V),$$

The joint pdf of U and ϕ, i.e., $f_{u\phi}(V, \psi)$, can be defined as,

$$f_{u\phi}(V, \psi) \equiv \frac{\partial^2}{\partial V \partial \psi} F_{u\phi}(V, \psi)$$

It must be considered that $F_{u\phi}(V, \psi)$ and $f_{u\phi}(V, \psi)$ exists in a two dimensional $V - \psi$ sample space. Following properties for joint pdf $f_{u\phi}(V, \psi)$ can also be defined as the same way [16] for joint distribution function as follows,

$$f_{u\phi}(V, \psi) \geq 0$$

$$\int_{-\infty}^{\infty} \int_{-\infty}^{\infty} f_{u\phi}(V, \psi) dV d\psi = 1$$

$$\int_{-\infty}^{\infty} f_{u\phi}(V, \psi) dV = f_{\phi}(\psi)$$

and

$$\int_{-\infty}^{\infty} f_{u\phi}(V, \psi) d\psi = f_{u}(V)$$

Similarly, one-point joint probability density function $f_{u\psi\Theta}(V,\phi,\Theta;x,t)$ for random variables' velocity field $V(x,t)$, thermo-kinetic scalar space $\phi(x,t)$ and the turbulent frequency $\Theta(\mathrm{x},\mathrm{t})$ with their respective sample space variables (V,ψ,ω) can be written as: -

$$f_{u\psi\omega}(V,\phi,\Theta)dVd\phi d\Theta = \mathrm{P}\{V \le u(x,t) \le V+dV, \phi \le \psi \le \phi + d\phi, \Theta \le \omega \le \Theta + d\Theta\}$$

Hence it also satisfies the general properties for PDF such as,

$$f_{u\psi\omega}(V,\phi,\Theta;\mathrm{x},\mathrm{t})dVd\phi d\Theta \ge 0$$

$$\int_{-\infty}^{\infty}\int_{-\infty}^{\infty}\int_{-\infty}^{\infty} f_{u\psi\omega}(V,\phi,\Theta;\mathrm{x},\mathrm{t})dVd\phi d\Theta = 1$$

If $t(u,\psi,\Theta;x,t)$ is a function of any of the random flow variables discussed above, its averaged value can be defined as follows,

$$\overline{t(x,t)} = \int_{-\infty}^{\infty}\int_{-\infty}^{\infty}\int_{-\infty}^{\infty} t(u,\psi,\Theta;x,t).f_{u\psi\omega}(V,\phi,\Theta;\mathrm{x},\mathrm{t})dVd\phi d\Theta$$

Similarly, Favre averaged quantity for $t(u,\psi,\Theta;x,t)$ can be obtained as,

$$\widetilde{t(x,t)} = \int_{-\infty}^{\infty}\int_{-\infty}^{\infty}\int_{-\infty}^{\infty} t(u,\psi,\Theta;x,t).\widetilde{f}_{u\psi\omega}(V,\phi,\Theta;\mathrm{x},\mathrm{t})dVd\phi d\Theta$$

where $\widetilde{f}_{u\psi\omega}(V,\phi,\Theta;\mathrm{x},\mathrm{t})dVd\phi d\Theta$ is the Favre-averaged PDF as given in [16].

4.3 Transported PDF Equation

The main objective for obtaining the probability density function (PDF) is to get the one-point statistical description such as mean, variance and co-variance [16,17]. As described in the previous section (4.2.2), if the one-point joint-composition frequency PDF given in section 4.2.2 is known, mean or Favre-averaged quantities can be easily determined [16].

The PDF transport equation described in [16] for a joint pdf $f(V,\psi;x,t)$ (in the above section) is:

$$\rho(\underline{\psi})\frac{\partial f}{\partial t}+\rho(\underline{\psi})V_j\frac{\partial f}{\partial x_j}+\left(\rho(\underline{\psi})g_j-\frac{\partial\langle p\rangle}{\partial x_j}\right)\frac{\partial f}{\partial V_j}+\frac{\partial}{\partial\psi_a}\left[\rho(\underline{\psi})S_\alpha(\underline{\psi})f\right]$$
$$=\frac{\partial}{\partial V_j}\left[\left\langle-\frac{\partial\tau_{ij}}{\partial x_i}+\frac{\partial p'}{\partial x_j}\middle|\underline{V},\underline{\psi}\right\rangle\right]+\frac{\partial}{\partial\psi_\alpha}\left[\left\langle\frac{\partial J_i^\alpha}{\partial x_i}\middle|\underline{V},\underline{\psi}\right\rangle\right]$$

The mean pressure $\langle p\rangle$ can be obtained from the Poisson equation [7] and $\rho(\psi)$ and $S(\psi)$ are known functions [16]. Thus, all the left-hand side terms are on closed side. Terms that need to be modelled (τ_{ij}, p' and J_i^α) will be explained in the next section (Particle Approach) except for the ones that are needed as the input.

Since the joint pdf does not provide any information about the time or length scales regarding capturing turbulence, this information needs to be provided as the input before solving the problem [16]. All the models involve a turbulent time scale $\tau(x,t)$ which is defined as [5,7,16],

$$\tau = k/\epsilon,$$

where k is the turbulent kinetic energy,

$$k=\frac{1}{2}\langle u_iu_i\rangle=\iint\frac{1}{2}(V_i-\langle U_i\rangle)(V_i-\langle U_i\rangle)f\,d\underline{V}\,d\underline{\psi},$$

and ϵ is the rate of dissipation of k,

$$\epsilon=\left\langle\tau'_{ij}\frac{\partial U_j}{\partial x_i}\right\rangle/\rho$$

The closure problem posed by RANS modeling described earlier (section 3.3.2) i.e., dealing of Reynolds averaged stresses $\widetilde{u_i''u_j''}$ can now be treated as the same way as done in section 4.2.2 for $f_{u\psi\Theta}(V,\phi,\Theta;x,t)$.It can be defined as,

$$\widetilde{u_i''u_j''}=\int_{-\infty}^{\infty}\int_{-\infty}^{\infty}\int_{-\infty}^{\infty}(V_i-\bar{u}_i).\left(V_j-\bar{u}_j\right).\widetilde{f}_{u\psi\omega}(V,\phi,\Theta)dV\,d\phi\,d\Theta$$

Similar expression for $\alpha-th$ thermo kinetic scalar space ($\widetilde{S_\alpha}$) [16] can be written as follows,

$$\widetilde{S_\alpha}=\int_{-\infty}^{\infty}\int_{-\infty}^{\infty}\int_{-\infty}^{\infty}S_\alpha(\phi).\,\widetilde{f}_{u\psi\omega}(V,\phi,\Theta)dV\,d\phi\,d\Theta$$

The averaging for highly non-linear terms is solved and hence no modelling is required. A more general way is to solve a transported PDF evolution equation [16] to obtain the instantaneous PDF $f_{u\psi\omega}(V,\phi,\Theta;\mathrm{x},\mathrm{t})$ at every location in the flow field. It is derived from Navier-Stokes equations and scalar conservation equation [16,17] and after the derivation presented in [16], it can be presented as follows,

$$\frac{\partial\bar{\rho}\tilde{f}}{\partial t}+\frac{\partial\bar{\rho}V_i\tilde{f}}{\partial x_i}-\left(\frac{\partial\bar{\tau}_{ij}}{\partial x_j}+\frac{\partial\bar{p}}{\partial x_i}\right)\left(\frac{\partial\tilde{f}}{\partial V_i}\right)+\frac{\partial\bar{\rho}S_\alpha\tilde{f}}{\partial\phi_\alpha}$$
$$=-\frac{\partial}{\partial V_i}\left\{\overline{\left(\frac{\partial\tau'_{ij}}{\partial x_j}-\frac{\partial\bar{p}}{\partial x_i}\middle|\,\Theta,V,\phi\right).\tilde{f}}\right\}+\frac{\partial}{\partial\phi_\alpha}\left\{\overline{\left(\frac{\partial}{\partial x_j}\left(D_\alpha\rho\frac{\partial\phi_\alpha}{\partial x_j}\right)\middle|\,\Theta,V,\phi\right).\tilde{f}}\right\}$$
$$-\frac{\partial}{\partial\Theta}\left\{\overline{\left(\frac{D\omega}{Dt}\middle|\,\Theta,V,\phi\right).\tilde{f}}\right\}$$

4.4 Particle Approach for transported PDF Equation

The transported evolution equation PDF described in the above section is an integral differential equation with $n+8$ variables (n being the thermo-kinetic scalars, 3 velocity components, 3 for physical space, turbulent frequency and time). The Monte-Carlo method for turbulent reactive flows [17] is found to be quite beneficial as compared to conventional methods such as Finite Element, Finite Difference and Finite Volume method [7,16,17].

The perfectness of Monte Carlo method in solving PDF evolution Equation comes from the finding [16,17] that the computational effort increases only linearly with the increasing dimensionality of sample space variable.

The position (or spatial location) and turbulent frequency are modelled using their respective governing equations as illustrated in [8,16,17] and will be explained in section 6.3. To model the thermo-kinetic scalar or composition space, different molecular mixing models that concentrate on the particle interaction within a particular cell are adopted. This will be explained in detail in section 5.

5. Molecular Mixing Models

5.1 Basic Concept

Modelling the conditional diffusion term in the transported PDF evolution equation is one of the major tasks in the PDF solver [16] as this term inherently describes the nature and accuracy of the molecular mixing process among the particles in a particular cell. It can be illustrated using the following expressions as below:

$$J_i = -\Gamma \frac{\partial \phi}{\partial x_i}$$

where ϕ is the molecular flux, $\langle \phi \rangle$ is the mean, with corresponding variance $\langle \phi'^2 \rangle$ and Γ being the constant diffusion coefficient. Consequently, its transport equation in context of random variable concept [16] can be presented as:

$$\rho \frac{D\phi}{Dt} = \Gamma \nabla^2 \phi$$

For the case considered,

$$\frac{\partial \langle \phi \rangle}{\partial t} = 0$$

signifying that mean $\langle \phi \rangle$ is constant. An equation for variance can be obtained [16] by multiplying eqn 15 by ϕ and then taking the mean,

$$\frac{1}{2} \frac{\partial \langle \phi^2 \rangle}{\partial t} = -\epsilon_\phi$$

where ϵ_ϕ is the scalar dissipation and can be defined as,

$$\epsilon_\phi = \left(\frac{\Gamma}{\rho}\right) \left\langle \frac{\partial \phi'}{\partial x_i} \frac{\partial \phi'}{\partial x_i} \right\rangle$$

which shows that variance continuously decays for $\epsilon_\phi \geq 0$.

As the time scale ratio ($\tau = k/\epsilon$) presents the decay of velocity fluctuations [16], similarly $\tau_\phi \equiv \frac{1}{2} \langle \phi'^2 \rangle / \epsilon_\phi$ is the decay time scale of scalar fluctuations. Detailed explanation for

ϵ_ϕ along with its derivation can be found in [16]. The both time scales ratio are related [18] to each other by a mixing model constant [19] as,

$$\tau_\phi = \tau / C_\phi$$

The value of this parameter (C_ϕ) changes for different mixing models [20-30]. Equation for variance can be derived [16] in its terms as,

$$\frac{\partial \langle \phi'^2 \rangle}{\partial t^*} = \langle \phi'^2 \rangle_o \exp(-C_\phi t^*)$$

where, $\langle \phi'^2 \rangle_o$ is the initial condition at $t_* = 0$.

The pdf of $\phi, f(\psi; t)$ (as in section 3.1) can be said to follow the gaussian condition if it satisfies the below expression.

$$f_\phi(\psi) = (2\pi \langle \phi'^2 \rangle)^{-\frac{1}{2}} \exp(-\frac{1}{2}[\psi - \langle \phi \rangle]^2 / \langle \phi' \rangle^2)$$

Evolution PDF equation can be derived [16] for $f_\phi(\psi; t)$ as,

$$\frac{\partial f_\phi}{\partial t} = -\frac{\partial}{\partial \psi}\left[f_\phi \left\langle \left(\frac{\Gamma}{\rho}\right) \nabla^2 \phi \middle| \psi \right\rangle \right]$$

It is quite evident that the evolution of the above equation depends on the term $\left\langle \left(\frac{\Gamma}{\rho}\right) \nabla^2 \phi \middle| \psi \right\rangle$ which needs to modelled. This term also takes the account of determination of flow variables in the composition space [17].

Different mixing Models with different pros and cons have been developed over past few decades [20-23] to overcome the modelling problem for this diffusion term. Interaction by Exchange with mean (IEM) [20] and Curl's Coalescence and dispersion (C/D) [21] model previously proposed are two basic ones which pose problems like relaxation to gaussian distribution, mixing in reference or composition space, conditional effects on mixing timescales and reference space as described in detail [8,11,19,22,29].

In the upcoming sections (4.2 and 4.3), detailed explanations for Modified Curl's model and Multiple Mapping Closure Model (Velocity Conditioned) (proposed in this thesis) will be described in each of the different section as MMC approaches have shown quite a significant improvement in the past few years [22,25-31].

5.2 Modified Curl's Model (MCM)

Modified Curl's model is the advanced implementation of the curl's Coalescence and dispersion model [21]. It is a stochastic model where a pair of unmixed particles in a particular CFD cell are selected randomly (using a PDF-MCD approach [30]).

To illustrate this, a rectangular cell like domain with 50 particles are considered to describe the particle selection adopted in MCM model. Consequently, particles with their default α and β values are distributed in $\alpha - \beta$ space where α, β can present either scalar or any other reference space. If 'p_1' is the one of the first particles selected randomly, it can be paired with a second unmixed randomly selected particle 'q_2' from the ensemble and become a pair (p_1,q_1).

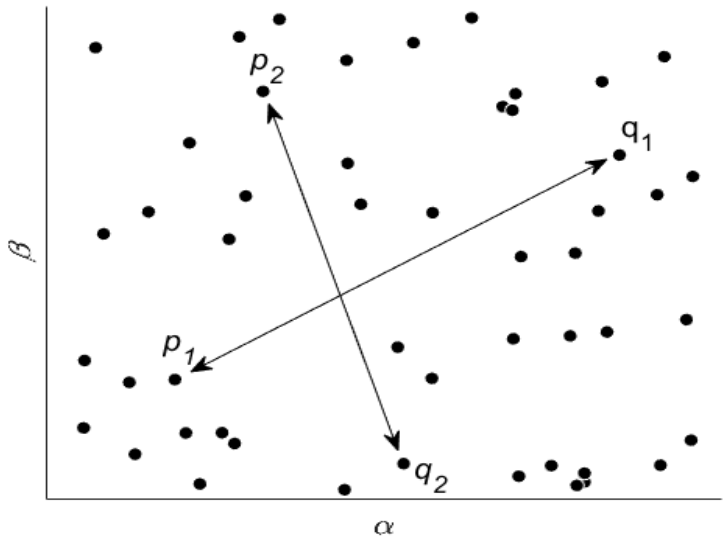

Figure 5: Particle Selection in MCM Model

It must be taken into consideration that the other set of pair which need to be selected randomly in the same fashion from the ensemble, does not need to be premixed. It means that it has to be from (N-2) remaining unmixed particles in the cell. This process in continued until there are no unmixed particles left in the cell. It can be illustrated in the Figure *5*.

The pair selected in the whole process is allowed to mix according to the following algorithm presented in [24,30],

$$\phi^{*,p}(t+\Delta t) = \phi^{*,p}(t) + \mu\left(\phi^{p,q}(t) - \phi^{*,p}(t)\right)\frac{\Delta t}{\tau}$$

$$\phi^{*,q}(t+\Delta t) = \phi^{*,q}(t) + \mu\left(\phi^{p,q}(t) - \phi^{*,q}(t)\right)\frac{\Delta t}{\tau}$$

where,

$$\mu = 1 - \exp\left(-\frac{w_p + w_q}{W}\frac{N}{2}\right) \approx \frac{w_p + w_q}{W}\frac{N}{2}$$

$\phi = \{Z, Y_1, Y_2 \dots \dots Y_n\}$ represents the scalar space, N is the number of particles within the cell, w_p, w_q are the weights of the pair of unmixed particles (ip, iq) selected directly from the ensemble, $W = \sum_{i=N}^{W} w_i$ (i.e., the sum of weight of all the particles in the ensemble),$\phi^{p,q}(t)$ is the weighted average of the particles pair (p, q) at a particular time instant t' given by

$$\phi^{p,q}(t') = \frac{(w_p\phi_p(t') + w_q\phi_q(t'))}{w_p + w_q}$$

Moreover, τ is the mixing timescale [18] given by the below equation, C_ϕ being the mixing parameter.

$$\tau = \frac{1}{C_\phi}\frac{k}{\epsilon}$$

The above algorithm is implemented in MM-INTAS library which was developed by group INTAS contributing to the INTAS project (www.instas.be) concerned towards the development of turbulent mixing models. The computer program was used as a tool to test the above micro-mixing models in context of lagrangian modelling. Evolution of composition PDF is obtained in a small domain where a frozen homogeneous turbulence exists, characterized by turbulence frequency 'ω' and is defined as the ratio of dissipation of turbulent kinetic energy to the turbulent kinetic energy. The evolution of the composition of each of the assigned particles in a cell at particular time step of 1e-03 evolves due to the mixing and chemical reactions. To illustrate the same, pictorial presentations of PDF of the mass fraction of methane ($P\left(Y_{CH_4}\right)$) have been plotted against the methane mass fraction (Y_{CH_4}) in the figure below,

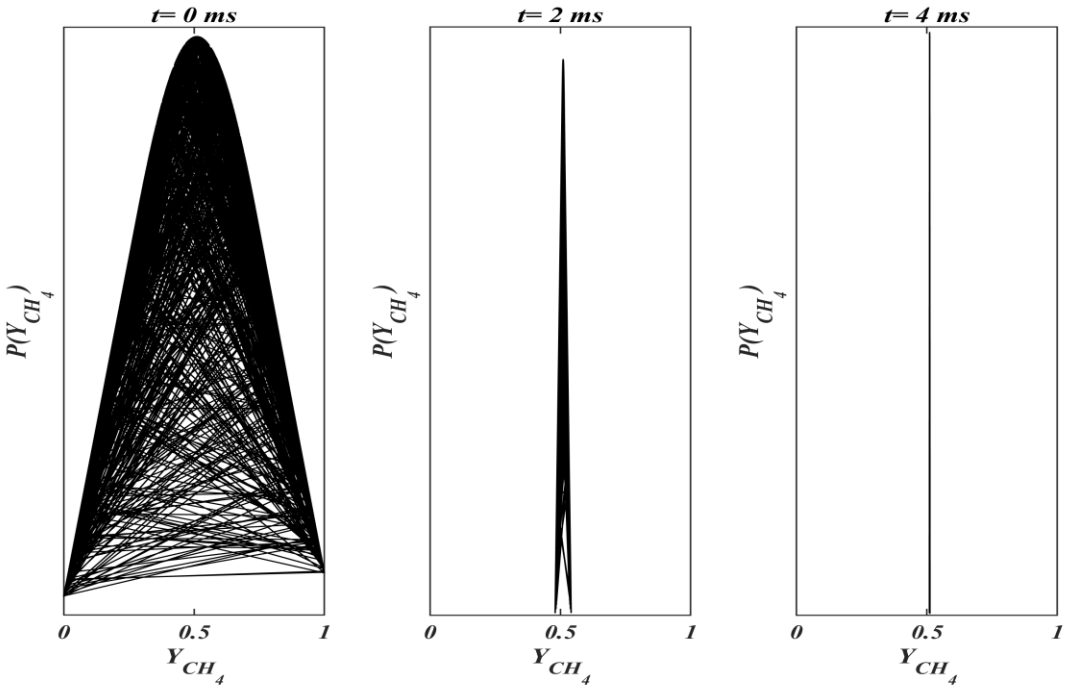

Figure 6:PDF Evolution in MCM Model

5.3 Velocity Conditioned Multiple Mapping Closure (VMMC)

Modified Curl's Model (MCM) described in the above section doesn't satisfy the localness in the composition or reference space [27,29,30,31] accounted by the random selection of particles from the ensemble. Multiple Mapping Closure Model uses reference variables simulating properties of the turbulent flow not only from the composition space but other fundamental quantities. The theory behind MMC lies behind the concept that particles must be selected that are close to each other in reference space [27,31] as presented in the figure below,

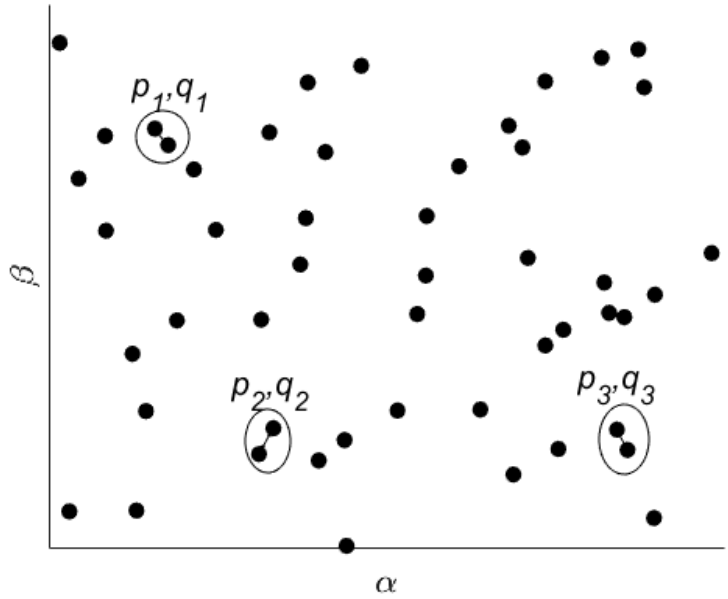

Figure 7: Particle Selection in MMC Model

The approach of adopting the mixture fraction like reference variable ξ [29,34] is used to determine what particles are permitted to mix. Alternatively, in the generalized MMC, magnitude velocity, fluctuating component of velocity, scalar dissipation, enthalpy or other combustion useful quantities can be taken as a reference variable [34-36].

The diffusion term which needs to be modelled is considered to be independent of the velocity statistics in the PDF model. Various implementations for mean conditioning models especially IE(C)M (Interaction by Exchange with conditional Mean) [32,33] earlier proposed takes the effect of velocity conditioning on the diffusion term. This physically means that particles with the nearest convection are allowed to mix accordingly in a particular cell.

Therefore, in this thesis, in order to take the velocity conditioning into effect, first the particles in a particular cell are sorted according to their mean velocity magnitude and then the neighboring particles are allowed to mix. Results will be compared between MCM and MMC models for further conclusions and to gain insights about the constructed logic.

6. Turbulent Non-premixed piloted Flames

6.1 Introduction

In non-premixed combustion, the fuel and oxidizer streams are mixed separately, and combustion occurs after the fuel and oxidizer mix on the molecular scale. Many practical combustion devices, such as furnaces, steam boilers, diesel engines, liquid rocket motors, gas turbine engines and scramjet engines involve turbulent non-premixed combustion. In these devices, mixing occurs by a combination of turbulent stirring of the fuel and oxidizer streams and molecular diffusion. Turbulence greatly enhances the mixing process by increasing the surface area of the thin mixing layers where most of the molecular diffusion occurs. The interaction between turbulent mixing and combustion chemistry is extremely complex and remains an active research area [15-30,40-44]. The emphasis is on fundamental phenomena that have been experimentally studied in relatively simple burner configurations but are also relevant to the understanding and predictive modeling of complex combustion systems.

Sandia Flame series D-F is a well-known flame for study of turbulent non-premixed flames [37,38] that will be discussed in the next section.

6.2 Methodology

Sandia Flame Series D-F consist of a fuel jet with diameter D =7.2 mm. The fuel is a mixture of 25% methane and 75% air by volume. The mixture is beyond the flammability limits and flame burn like a diffusion flame. The jet is surrounded by the co-axial pilot with an outer diameter $D = 18.2\text{mm}$ with a mixture of C_2H_2, air, CO_2 and N_2 and is operated at a fuel lean condition with equivalence ratio of 0.77 with its regular thermodynamic properties. Experimental studies were conducted by Barlow and Frank [37]. However, in this work only Sandia Flame Series D will be studied due to the numerous reasons. First, a detailed experimental database in available online [37,38,43] that makes it possible to judge merits or demerits of the new method. Second, it has been the object for numerous modeling attempts for PDF simulations [39]. Last but not the least, this flame exhibits very low levels of local extinction [29,30] hence fulfilling the need to have a valid platform to test different mixing

models. Sandia Flame D has a Reynolds number of 22,400 for the jet corresponding to the jet velocity of 49.6m/s.

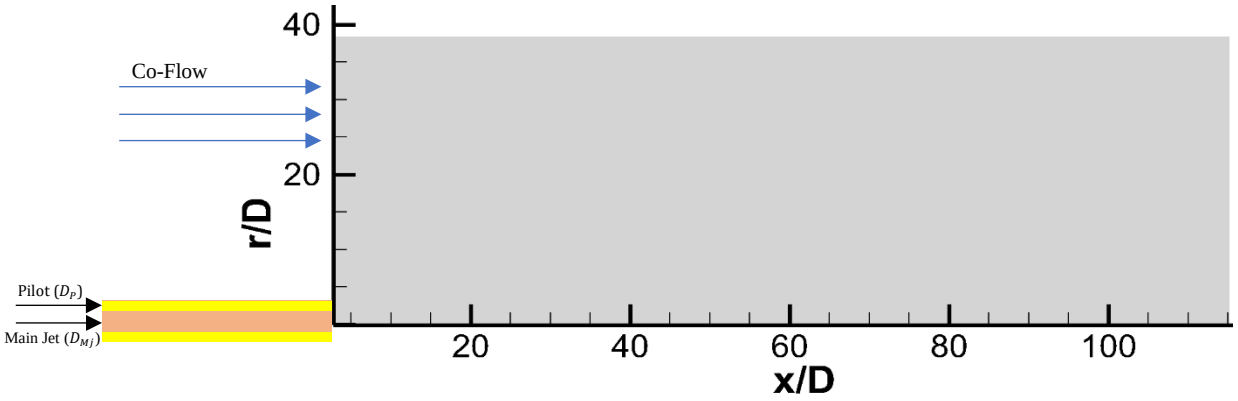

Figure 8: Computational Setup for Sandia Flame D

Computational domain or flame is used in an axi-symmetric case to reduce the computational efforts across the axial direction. Proper boundary conditions are used in order to eliminate pipe of the domain. Simulation is performed with a domain with dimensions 120D (axial) x 40D (radial) hence with a good agreement with the experimental wind tunnel configuration [37] discretized by a total of 1500 cells. A grid sensitivity study has demonstrated sufficient resolution for the RANS flow and mixing fields.

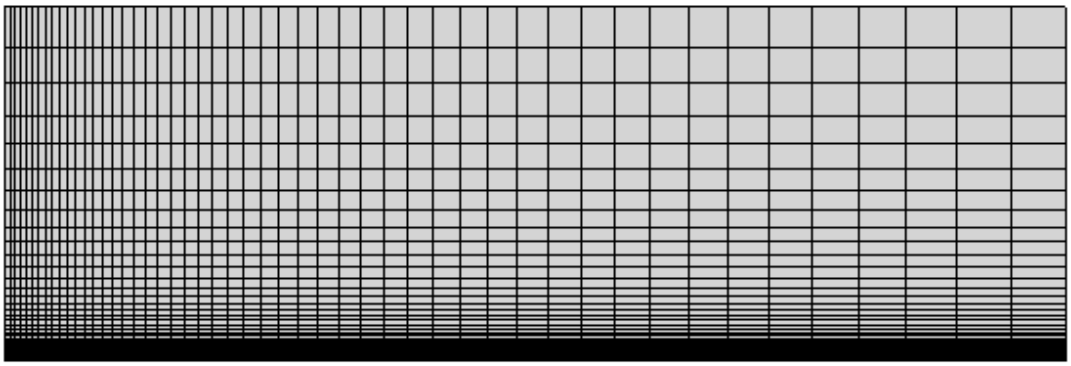

Figure 9: Grid for Sandia Flame D

Boundary Conditions are provided on the jet exit plane at $x/D = 0$ as they are readily provided in [44]. The mean axial velocity [44], Reynolds stresses ($\widetilde{u_1''u_1''}$, $\widetilde{u_2''u_2''}$, $\widetilde{u_1''u_2''}$) which are conditioned in a good agreement with [45].Turbulence frequency at the inlet along with its variance are adopted as in [45]. Last, the ratio of dissipation of turbulent kinetic energy k is specified as unity.

Boundary conditions for the thermo-kinetic or the composition state (with a limited number of species) is provided as shown in the table below. Thermodynamic properties for the main jet were respectively taken as 294 K (Temperature), 1 Bar (Pressure) with a mixture of 25% CH_4 and 75% dry air. The co-flow consists of pure dry air with a temperature of 292 K and pressure of 1 bar. The pilot composition at the inlet can be a mixture of CH_4/air premixed flame with an equivalence ratio of 0.77. An inlet profile of 1880K and 1 bar is considered in validation with the experimental measurements [45].

Scalar/Inlet Profile	Main-jet	Co-flow	Pilot
H	-725.7 Kj/Kg	-7.18Kj/Kg	-206.7 J/Kg
p	1 Bar	1 Bar	1 Bar
ϕ_{N_2}	23.21mol/Kg	27.30 mol/Kg	26.22 mol/Kg
ϕ_{O_2}	6.088 mol/Kg	7.35 mol/Kg	1.65 mol/Kg
ϕ_{CO_2}	0.0 mol/Kg	0.0 mol/Kg	2.50 mol/Kg
ϕ_{CH_4}	9.66 mol/Kg	0.0 mol/Kg	0.0 mol/Kg
ϕ_{OH}	0.0 mol/Kg	0.0 mol/Kg	0.17 mol/Kg

Table 1: Thermo-Kinetic States for various inlet profiles

6.3 Solution Procedure

6.3.1 Hybrid FV/PDF Method

In Fig, the flow chart of the hybrid algorithm developed at ITT-KIT is presented. Initially, Finite Volume Method [6,7] with particle method code are initialized with the initial conditions and boundary conditions. FVM is performed to obtain the Favre-averaged density $\bar{\rho}$ and $\tilde{u}$ for each of the cells, which are further used as an input in PDF particle method. A particular no. of particles (user input) is assigned to each CFD cell in the discretized domain. Each particle constitutes its own position in physical space x^*, velocity fluctuation u'', turbulent frequency ω^* and the progress variable φ^*. Each of the particle's progress variable is passed into the REDIM interface which acts as a reduced chemistry code and feed backs the updated progress variable and Temperature T^* at the time $t + \Delta t$ to the particle code. In the next step, velocity fluctuation u'' and Temperature T^* is known for each particle. Thus, all the particles belonging

to a particular cell contribute towards calculating the Favre-averaged Reynolds stresses $\bar{\rho}\widetilde{u_i''u_j''}$ and temperature at this cell center. Afterwards, time averaging is applied to all Favre averaged quantities to reduce the statistical errors. Then the updated time-averaged temperature $\tilde{T}$ is used or determination of the averaged pressure by ideal gas equation given by,

$$\bar{p} = \bar{\rho}.\widetilde{R_g T}$$

Thus, it eliminates the use of Poisson equation [3,7] to be used for correcting the vector field. This updated pressure and other time-averaged quantities are fed back again into FVM code for the next iteration. The process is iterative until the desired number of iterations are reached. For a better and more detailed explanations along with the coupling or projection methods used to deal with Reaction Diffusion Manifolds (REDIM) interface, reader is referenced to [8,46].

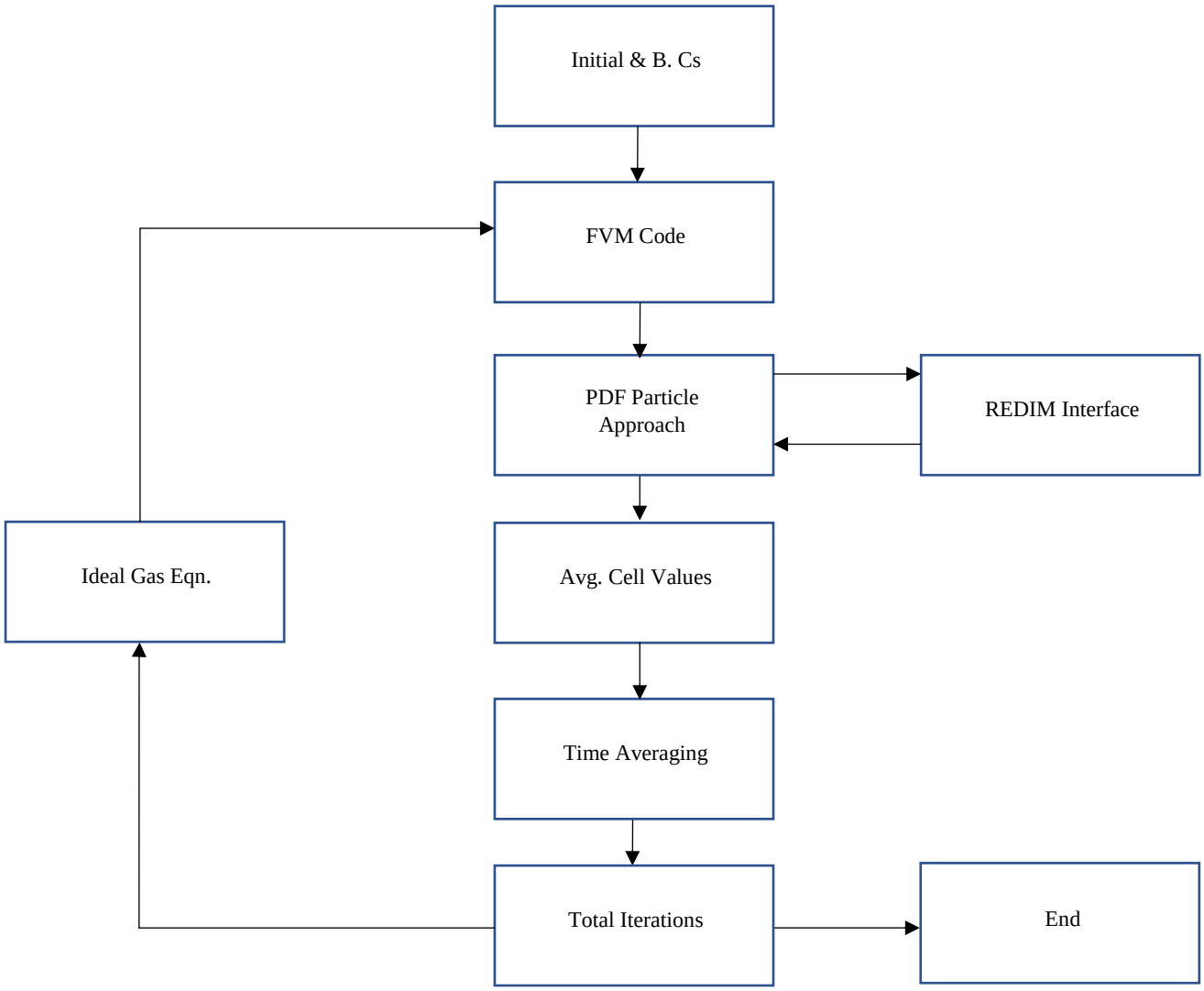

Figure 10: Flow Chart for Solution Procedure for the Hybrid FV/PDF Method

6.3.2 Numerical Implementation

In this sub-section, the numerical implementation of the above hybrid FV/PDF Method is briefly explained. First of all, finite volume method as described [7,14] is used to present partial differential equation for all the conservations equations (compressible Navier-Stokes Equations) as described in section 3.3. The scheme adopted is an explicit Runge-Kutta Method [7,14] with an accuracy of 4^{th} order in time. A flow charted has been illustrated in Figure 11 below. For detailed theory behind this method, reader is advised to go through these references [7,8,14].

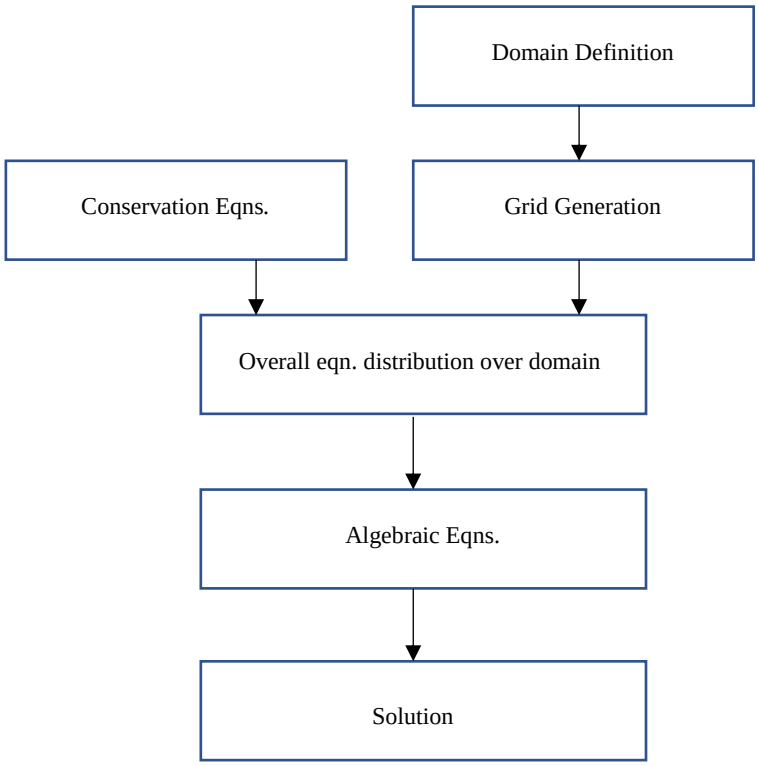

Figure 11:General Implementation for Finite-Volume Method

The averaged density $\bar{\rho}$ and Favre-averaged velocity $\tilde{u}$ are extracted from FVM and fed into the PDF particle code for further advancement in the algorithm. As discussed in the section 4.3, particle state can be determined by its position, velocity fluctuation, turbulent frequency and its mixing and reactions with other particles. Each of them will be described in this section briefly.

Particle Position

Particle position in a particular CFD cell is given by the following equation,

$$\frac{\partial X^*}{\partial t} = \tilde{u}(X^*) + u''$$

Integrating the above equation over an interval of $\Delta t/2$ from $t_n \rightarrow t_{n+\frac{1}{2}}$ through,

$$X^*_{t_{n+\frac{1}{2}}} = X^*_{t_n} + \left(\tilde{u}^*(t_n) + u''^*(t_n)\right).\frac{\Delta t}{2}$$

hence giving its position at time $t_{n+\frac{1}{2}}$.

A flow chart can be presented for a single time-step during the implementation of the whole algorithm in the *Figure 12*. After the integration through whole the process, particle's position at t_{n+1} can be calculated as follows,

$$X^*_{t_{n+1}} = X^*_{t_n} + \left(\tilde{u}^*(t_n) + u''^*(t_n)\right).\frac{\Delta t}{2}$$

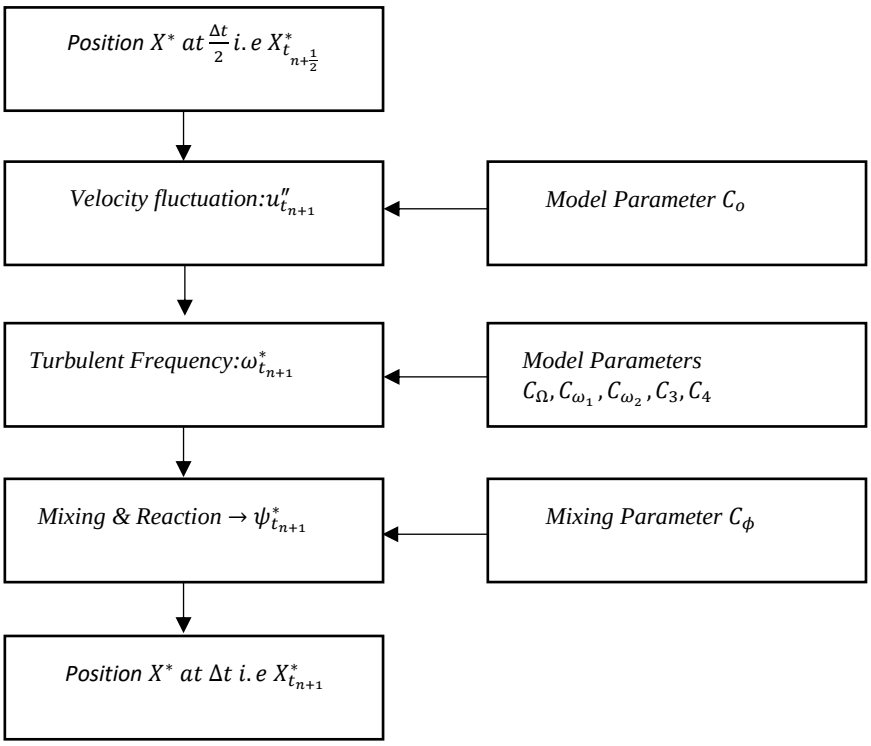

Figure 12: Numerical Implementation for FV/PDF Method

Particle Velocity Fluctuation

Particle Velocity can be known using the Simplified Langevin Model (SLM) as proposed in [16]:

$$du_i^*(t) = -\frac{1}{\bar{\rho}}\frac{\partial \bar{p}}{\partial x_i}dt - \left(\frac{1}{2}+\frac{3}{4}C_o\right)\Omega(u_i^*(t)-\tilde{u}_i)dt + \sqrt{C_o k\Omega}\,dW_i$$

where Ω and k are respectively the Favre averaged turbulent frequency and turbulent kinetic energy. Since, Favre-averaged is known from the RANS, it is recommended to use velocity fluctuation along with modified Simplified Langevin models [16,48].

$$du_i^{*\prime\prime}(t) = -\frac{1}{\bar{\rho}}\frac{\partial(\overline{p}u_i''\widetilde{u_j''})}{\partial x_i}dt - u_j''^*\frac{\partial u_j''}{\partial x_j}dt - \left(\frac{1}{2}+\frac{3}{4}C_o\right)\Omega(u_i^{*\prime\prime}(t)-\tilde{u}_i)dt + \sqrt{C_o k\Omega}\,dW_i$$

Therefore, particle's position can be determined by equation for X^* as stated above.

For its numerical solution, above equation can be integrated within a time interval (Δt) as follows,

$$\Delta u_i''^{,*} = \left(a_i + b_{ij}.u_j''^{,*}(t_n)\right).\Delta t + \sqrt{c.\Delta t}.\xi_i^u,$$

thus, giving the fluctuation as the time t_{n+1} as,

$$u_i''^{,*}(t_{n+1}) = u_i''^{,*}(t_n) + \Delta u_i''^{,*} + \frac{1}{2}b_{ij}.\Delta u_i''^{,*}.\Delta t,$$

where a, b, c are notations described [8] in the equation for $\Delta u_i''^{,*}$ described above.

Particle Turbulent Frequency

Since turbulent frequency to take proper time-scales into account, stochastic model for $\omega^*(t)$ proposed in [49] is used,

$$d\omega^*(t) = -C_3(\omega^* - \widetilde{\omega})\Omega dt - S_w\Omega\omega^* dt + \sqrt{2C_3C_4\widetilde{\omega}\Omega\widetilde{\omega}}dW$$

where S_ω is the source for turbulent frequency defined as,

$$S_\omega = C_{\omega 2} - C_{\omega 1}\frac{P}{k\Omega}$$

$C_3, C_4, C_{\omega 1}$ and $C_{\omega 2}$ are respectively the model parameters, values for C_3 and C_4 being 1.0 and 0.25 as in [16,49] but values for $C_{\omega 1}$ and $C_{\omega 2}$ depend upon the case which is being investigated. P is the turbulence production calculated as in [16,49]:

$$P = -\widetilde{u_i'' u_j''} \frac{\partial \widetilde{u}_i}{\partial x_j}$$

Molecular Mixing

For the particle mixing and reaction, the following equation can be integrated at each time step,

$$\frac{d\varphi^*(t)}{dt} = M^* + S(\varphi^*)$$

for which the nomenclature can be found in section 4. After integration, the above equation results as,

$$\varphi^*(t_{n+1}) = \varphi^*(t_n) - [\hat{S}(\varphi^*(t_n) + \widehat{M}^*(\rho^*(t_n))]dt$$

REDIM tables eases in the way that at every time-step, chemical source terms can be extracted from them thus eliminating the requirement of any further step in the process. The projection methods which have been described in detail [8,49] are used to give a proper evolution of the particle in thermo-kinetic state which follows several sub-steps for which reader is referenced to [8,49] for detailed explanations. REDIM uses the mass fraction of N_2 (Y_{N_2}) and mass fraction of CO_2 (Y_{CO_2}) as the reduced coordinates to represent the mixing state and reaction progress. REDIM lookup tables are then used to determine other scalars such as chemical species, temperature and density. Unity Lewis Number (ratio of thermal to mass diffusivity) assumption [1,3] is used in this methodology.

7. Turbulent Partially Premixed Piloted Flames

7.1 Introduction

Partially-Premixed Combustion is classified as the form of combustion in which incomplete mixing of fuel and the oxidizer takes place in the reaction zone. Inhomogeneity is common in most combustion devices such as Gas Turbine Engines where fuel injection is a little upwards of the swirling airflow from the compressor [50-52], gasoline direct injection engines where various methods are deployed to improve spark ignition, efficiency and as low emissions as possible[53], diesel or IC engines where processes occur in the premised zone with a diffusion flame [55] and industrial burners where turbulent sprays are lifted to counter direct contact with the burner [55]. Large Eddy Simulation (LES) is a great tool for analyzing turbulent combustion [57,62] but due to limited computational resources for this work, only RANS and Finite Rate Chemistry have been adopted.

In this work section, the well-known Sydney flame [56-60] operated under partial premixed conditions is simulated in Ansys Fluent under a single setup condition from the cases experimented in [56]. Experiments were conducted by Barlow [56], in which the line-imaged measurements of temperature and major species based on Rayleigh/CO-LIF techniques, are used to study and validate the behavior of species at different axial locations.

7.2 Numerical Setup and Methodology

Various cases had been studied under different setup conditions for the burner in [56] but in this work only one case with a nominal Reynold's number of 26,800 i.e., **FJ200-5GP-Lr75-57** will be studied.

The burner shown in the Figure 13 consists of two concentric pipes surrounded by the pilot with an inner diameter of 18 mm and a 0.2 mm wall thickness. The inner or central retractable main jet tube has an inside diameter of 4mm with a wall thickness of 0.25mm and serves as the inlet for fuel. The main tube or the annulus tube has an inside diameter of 7.5mm and a wall thickness of 0.25mm acting as the air inlet. The volumetric ratio V_A/V_F for air-fuel is 2.0. The burner is setup up in the wind tunnel with a square cross-section of 15 x 15 cm.

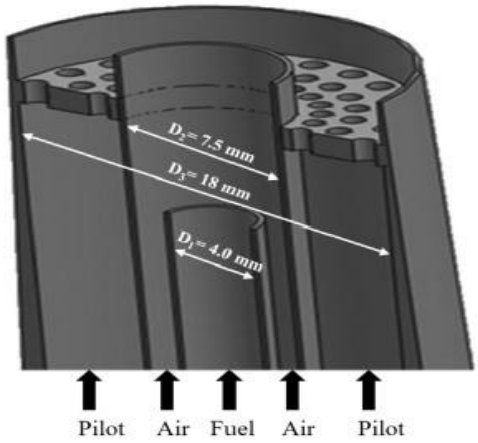

Figure 13: Burner Configuration with different inlet profiles

200 in the case name represents the volumetric air-fuel ratio of 2.0. 5 Gas Pilot (or '5GP') represents the mixture of 5 components (C_2H_2, H_2, CO_2, N_2 and air) for the pilot in proper proportions to match the stoichiometric mixture of CH_4/air with an adiabatic flame temperature of 2226K. 'FJ' represents the injection of fuel through the central tube and air in the annulus .Two digit numeric (75) with its Coefficient as 'Lr' is the recessed distance of the main jet tube or fuel inlet.

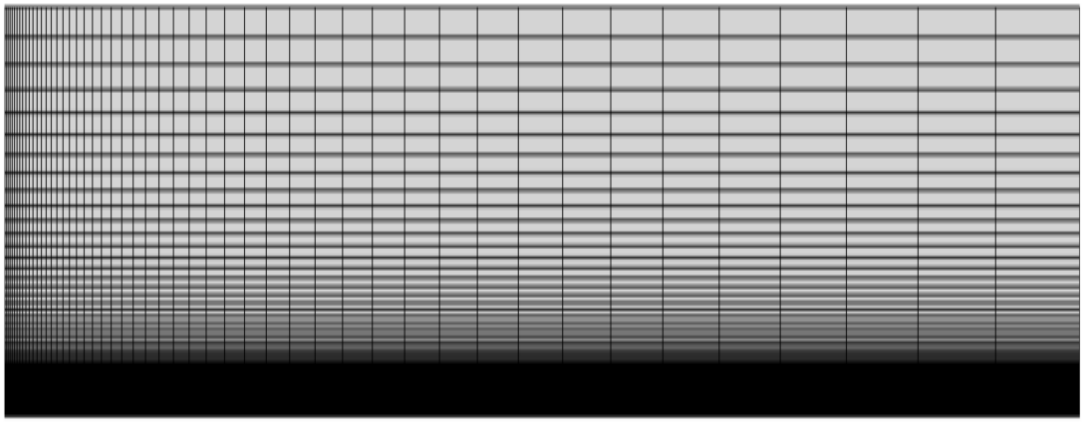

Figure 14: Grid for Sydney Flame

The case is treated as the axi-symmetric in nature with no swirl component for velocity. Computational domain was extended to 100 and 20 times in the axial and radial direction respectively. The grid was generated in ICEM-CFD with proper refinement across inlets for fuel, air and pilot.

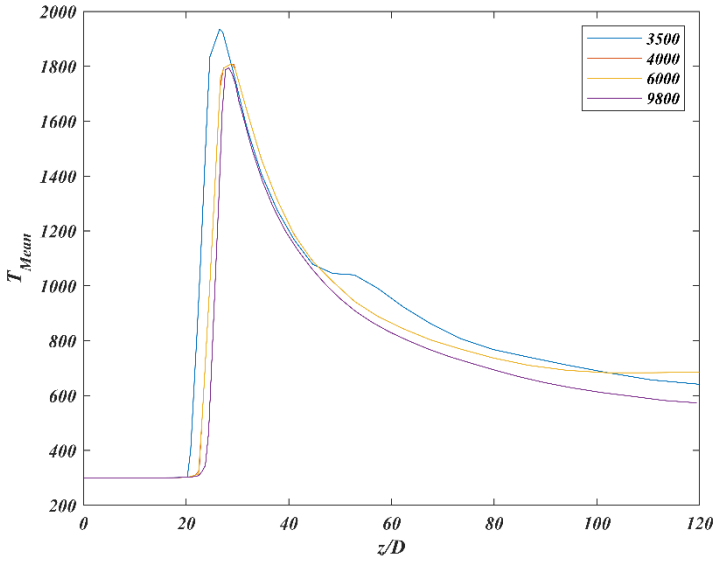

Figure 15: Grid sensitivity test for Sydney Flame

Mean temperature across the centerline in the axial direction was monitored with the solution procedure specified in section 7.3 for each of the grid size and a grid sensitivity test helped in finalizing a mesh of 4000 elements as shown in Figure 15.

7.3 Solution Procedure

The standard $k-\epsilon$ turbulence model is used as the RANS model with Finite Rate Chemistry [1,3,5]in Ansys Fluent incorporated with compressible Navier Stokes (density based Navier Stokes as termed by Ansys Fluent) solver. GRI 3.0 mechanism [45] is adopted for chemical kinetics with 27 species and 159 reactions without NO_x and soot.

Boundary conditions were imposed for co-flow, fuel, air and pilot inlets as in Table 2,

Phase/Species	Y_{CH_4}	Y_{O_2}	Temperature (in K)	Velocity (in m/sec)
Co-Flow	0.0	0.233	300	15
Fuel Inlet	0.055	0.217	300	67.0
Air Inlet	0.0	0.233	300	59.5
Pilot Inlet	0.055	0.233	2226	25.6

Table 2 : Inlet Boundary Conditions for Sydney Flame

The integral length scale was prescribed as 1/8th of the main tube diameter, 0.07 of the hydraulic diameter in the pilot and from L = κy in the co-flow (κ = 0.41) is the von Karman constant and y is the perpendicular distance from the pilot surface.

Upper wall was conditioned with no-slip condition and pressure outlet with 0-gauge pressure. The coupling of pressure and velocity is done through SIMPLE Algorithm to avoid any complexities in order to have a statistically stable and convergent solution. Spatial discretization for energy, momentum and all the species have been through second order upwind scheme [7] hence making them 3rd order accurate throughout the simulations, while for pressure, turbulent kinetic energy and dissipation rate was through 1st order upwind scheme, hence 2nd order accurate. Least Squares method was used for the gradient treatment in the upwind schemes. The convergence criteria were set to 0.0001 for continuity and momentum equations. Hybrid Initialization was used as an initialization method to initialize all the cell values. Instantaneous values for mean temperature (T_{Mean})and carbon dioxide mass fraction (Y_{CO_2}) were monitored at each different probe locations including the complete outlet until a constant stationary and convergent solution is obtained before they can be post-processed.

8. Results and Discussions

8.1 Sandia Flame D

The methodology described in section 6 is implemented for Sandia Flame D series. This section highlights the results obtained from implementation of MCM and VC-MMC model coupled with Hybrid FV/PDF method.

8.1.1 Sensitivity to number of particles

Each CFD cell contains a particular number of particles which plays a major role in determining the accuracy and extent up to which a particular mixing model can be used for determining the thermo-kinetic space. Each proposed model in recent times [20-23] is sensitive to number of particles and shows significant and distinguishable variations in mean and rms values of scalar quantities [19]. Therefore, for this purpose, checking the mixing model's sensitivity to this number poses a major task. Sensitivity of the mixing model is studied by drawing conclusions from variations in mean, rms and conditional averages values for a particular mixing timescale ratio and turbulence model in order to have a known value for how much particles must be reasonable for further simulations. The root mean square (rms), mixture fraction (ξ_{rms}), Mean temperature (T_{Mean}) along the centerline in axial direction, and Cond Avg Mean temperature w.r.t mixture fraction ξ are examined for an overview to finalize an exact number. These quantities are measured and analyzed for {20,50,80,100} particles per cell turn by turn for MCM and {20,50,100,200} for VC-MMC model respectively.

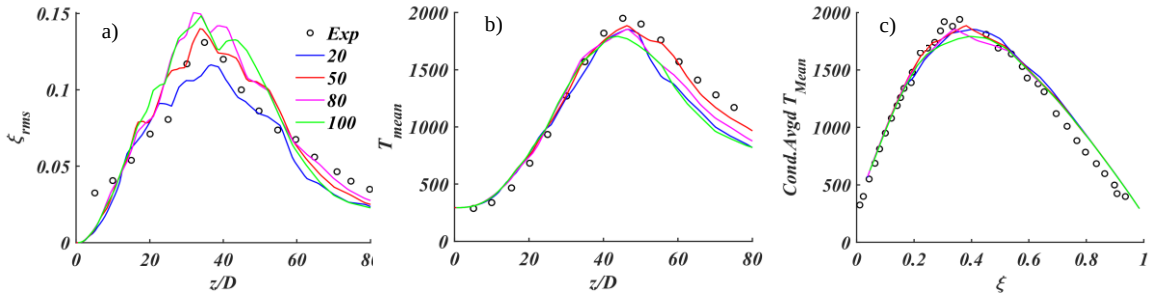

Figure 16: rms mixture fraction along the centerline in axial direction (a) Mean temperature along the same (b), and conditional averaged mean temperature w.r.t mixture fraction (ξ) (c) for MCM Model

For the Modified Curl's Model, it is evident from Figure 16 (b) that mean temperature along the centerline predicts with an excellent agreement of the experimental results with 50 particles/cell which is having the least deviation from the experimental data far downstream in the axial direction as comparison with all other cases. 20/cell predicts well till mid-centerline but declines away with the major dip afterwards. Taking ξ_{rms} into consideration (Figure 16(a)), large sensitivities can be observed from each other's prediction especially in the region covered from *z/D*=30 & *z/D*=50. Results for 50 matches well within this region against the experimental data although 80's results don't have a large difference from that of 50's but from Figure 16 (c) 50 seems can be concluded to be as the final one. For the conditional Averaged mean temperature, almost all are insensitive thus making 50 particles per cell to be a best choice for MCM model and further analysis.

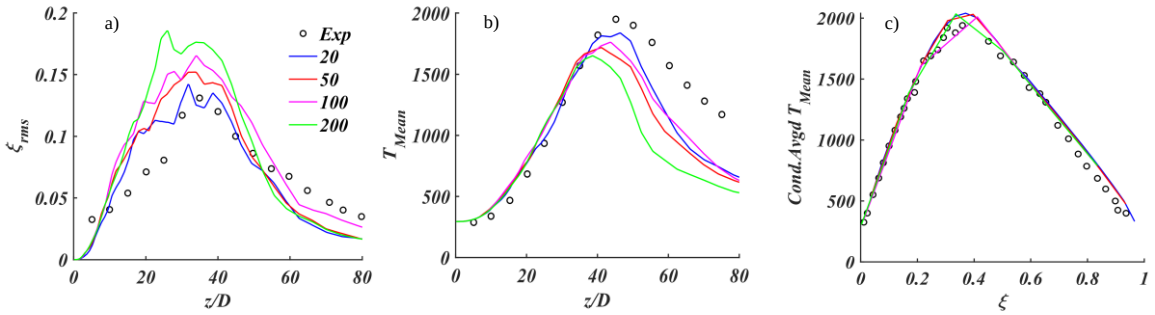

Figure 17 : rms mixture fraction along the centerline in axial direction (a) Mean temperature along the same (b), and conditional averaged mean temperature w.r.t mixture fraction (ξ) (c) for VC-MMC Model

On the other hand, for Velocity Conditioned Multiple Mapping Closure (VC-MMC) Model, consequently 20 particles /cell is concluded to be the best one. In Figure 17 (b) mean temperature values for 20's can be better compared to experimental data as compared to others. Not only that, ξ_{rms} values in 30-50 z/D region reaches the same peaks for 20/cell as compared well with those of experiments (Figure 17 (a)). Moreover, not much differences are observed (Figure 17 (c)) for cond. avgd. temperature as thereby proving 20 particles /cell as the best choice for this model.

8.1.2 Mixing Parameter Sensitivity Analysis

Values for Mixing Parameter often denoted by C_ϕ changes from model to model used in PDF calculations as illustrated in [19]. Each model is sensitive to its predictions within a specific range. C_ϕ for MCM model is taken as 3.8 as specified in [30]. In this section, for prediction of best value for VC-MMC model, a proper sensitivity analysis has been done. ξ_{rms} (rms mixture fraction), burning Index (BI) (for flame extinction), Y_{NO} (Nitrogen Monoxide mixture fraction) have been previously considered [19] to predict the nominal value of mixing parameter. However, in this work, only ξ_{rms} and Y_{NO} have been analyzed along the axial direction

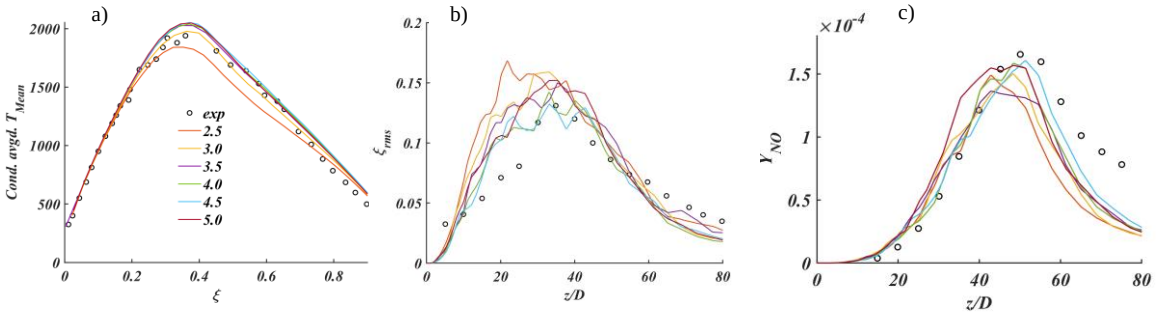

Figure 18: C_ϕ Sensitivity Analysis for VC-MMC model. Conditional averaged mean temperature w.r.t mixture fraction (ξ) (a), rms mixture fraction (ξ_{rms}) along the centerline in axial direction (b), and Y_{NO_2} along the same (c).

(centerline position) to study the effect of mixing parameter for this model. Averaged Conditional Mean Temperature w.r.t mixture fraction ξ is also considered to study the variations across conditional quantities.

As observed in Figure 18 (a) the peak of cond. Avgd. Mean temp is seen to increase with increase in C_ϕ, with no significant change in the values after 3.5, thus giving an ideal range of 3.5 and above. In the Figure 18 (b), it is quite evident that for rms mixture fraction (ξ_{rms}), each value seems fluctuating from another with a notable deviation from the experimental results especially in the region between *z/D=20* and *z/D=40*. Results for C_ϕ with value 4.5 are in good agreement with that of experimental data. Also, simulation results for 4.5 is also the best out of all in Y_{NO_2} case thus it is finalized for all the further simulations.

8.1.3 General results and observations

To study and check the behavior and accuracy of VC-MMC model, mainly scalars quantities such as species mass fractions (including mixture fraction) and temperature (Avg. and rms) are analyzed at different locations. Moreover, the conditional averaged quantities (conditioned on mixture fraction ξ) which are studied w.r.t mixture fraction and will be described later in this section.

Mean or time averaged results

First, the mean values are shown across the centerline (r/D = 0) in the axial direction and observations are shown in direction Figure. In context of 20 particles per cell, MMC model takes less computational effort than MCM model taking approximately 4 hours to reach a converged solution on a single core. It took around 75,000 iterations as compared to 3,50,000 for MCM (8-9 hours on the same machine) to reach convergence. It is evident that particle selection for mixing on the basis of their velocities takes less iterations than random selection from the ensemble. Nevertheless, sorting particles too takes additional computational efforts that can't be ignored and need to accounted for.

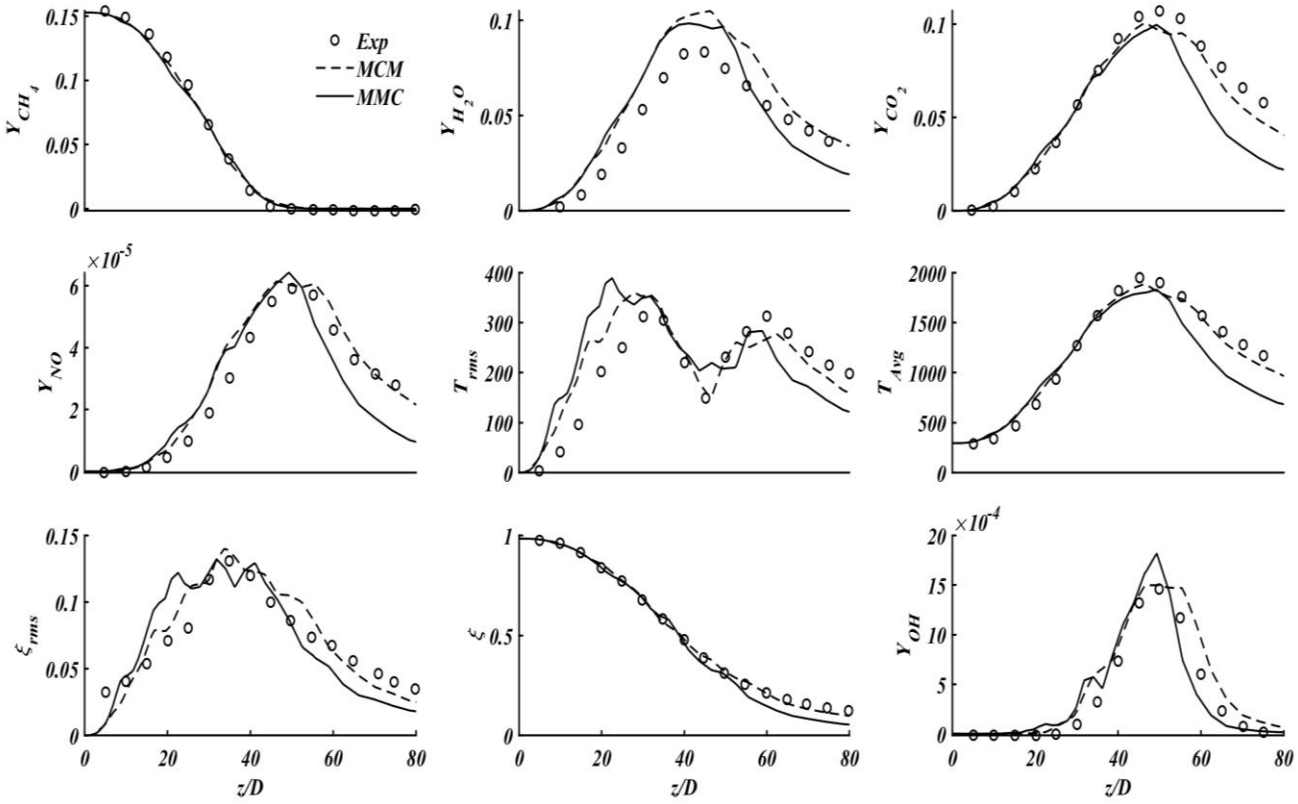

Figure 19: Temperature and species mass fraction along centerline in the axial direction

All the major mean scalar quantities are plotted along the centerline as shown in Figure 19. All the simulation results are in well agreement with the experimental data. Mass fraction for Methane (Y_{CH_4}) is almost accurately predicted for by both the models. Prediction of Y_{H_2O} is 20 % higher than that of experimental in different regions. Both the models show the same behavior till $z/D = 40$, MMC model predicting it well till $z/D = 60$ and further MCM till $z/D = 80$. Case of Y_{CO_2} seems to be opposite to that of Y_{H_2O} as it is observed to be

underpredicted. Though MCM model predicts it well at further downstream than MMC model (of which the rate of underpredicting goes on increasing). This same scenario is followed by both in case of Avg. Mean Temperature and Y_{NO}. However, Y_{NO} remains a little bit over and under predicted throughout the centerline. Fluctuations in predictions for T_{rms} and ξ_{rms} are commonly observed. However, MMC is observed to give better predictions for ξ_{rms} and Y_{OH} except at the peaks i.e. at $z/D = 50$. Underprediction of results in also noted in case of mixture fraction for MMC after $z/D = 60$.

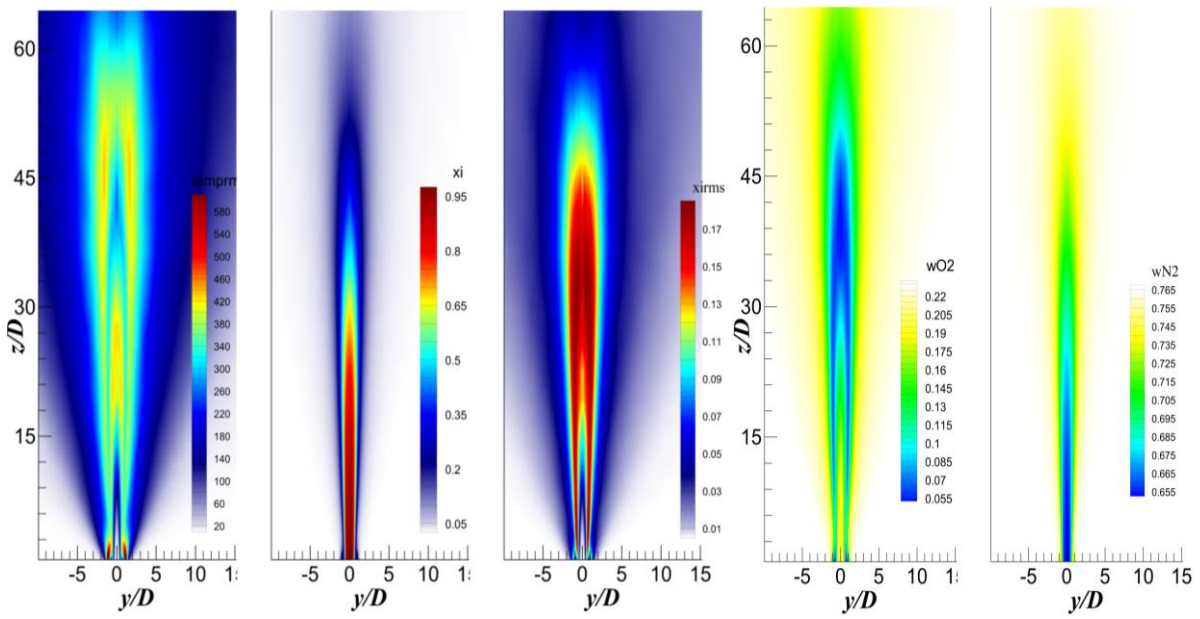

Figure 20: Contour presentations for root means square temperature, mixture fraction and rms mixture fraction (a) Mass fraction for Nitrogen and oxygen (b)

The comparison of radial profiles of the major scalar quantities also show good agreement with the experimental results and does not show any significant difference posing the need to present here and hence have been omitted from this work.

2D contour plots (only for MMC Model) for rms temperature and mixture fraction (rms & mean) in Figure 20 (a), Y_{N_2} and Y_{O_2} (Figure 20 (b)) and chemical species (with mean temperature) discussed have been presented further (Figure 21). All the quantitates are presented to be as fully converged and a stable solution. It is obvious from the plots that effects in the flow field for scalars such as mean temperature, Y_{CO_2} *and* Y_{H_2O} are observed for the radial direction y/D = -5 to 5. Although they are the products when the fuel is burnt and can be expected to show this much variation. Other scalars are mainly confined from region y/D = -2 to 2.

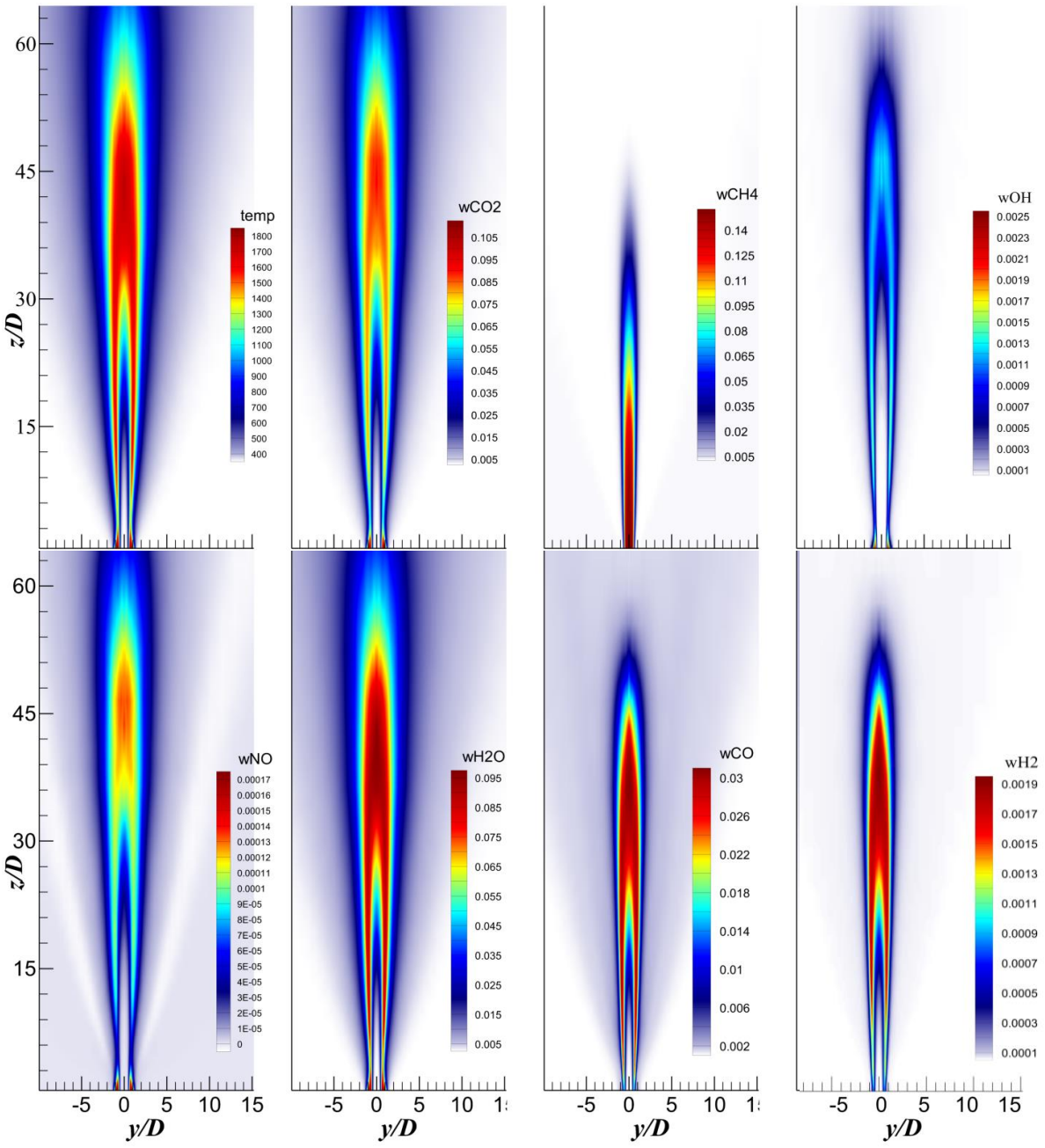

Figure 21:Contour presentations for mean temperature and mass fractions for major chemical species

Conditional Averaging

Although the results shown are quite interesting in determination of the structure of turbulent flames, they only give a description of time-averaged quantities. Another important aspect is the conditional averaging of these quantities on basis of mixture fraction which provide a better overview of turbulence-chemistry interactions. Scatter plots for selected species are shown in Figure *22* at the axial location of $z/D = 30$ for MMC model. Scatter plots provide the statistical description for a particular scalar and provide an overview of local extinction and repetitive ignition as described [8].

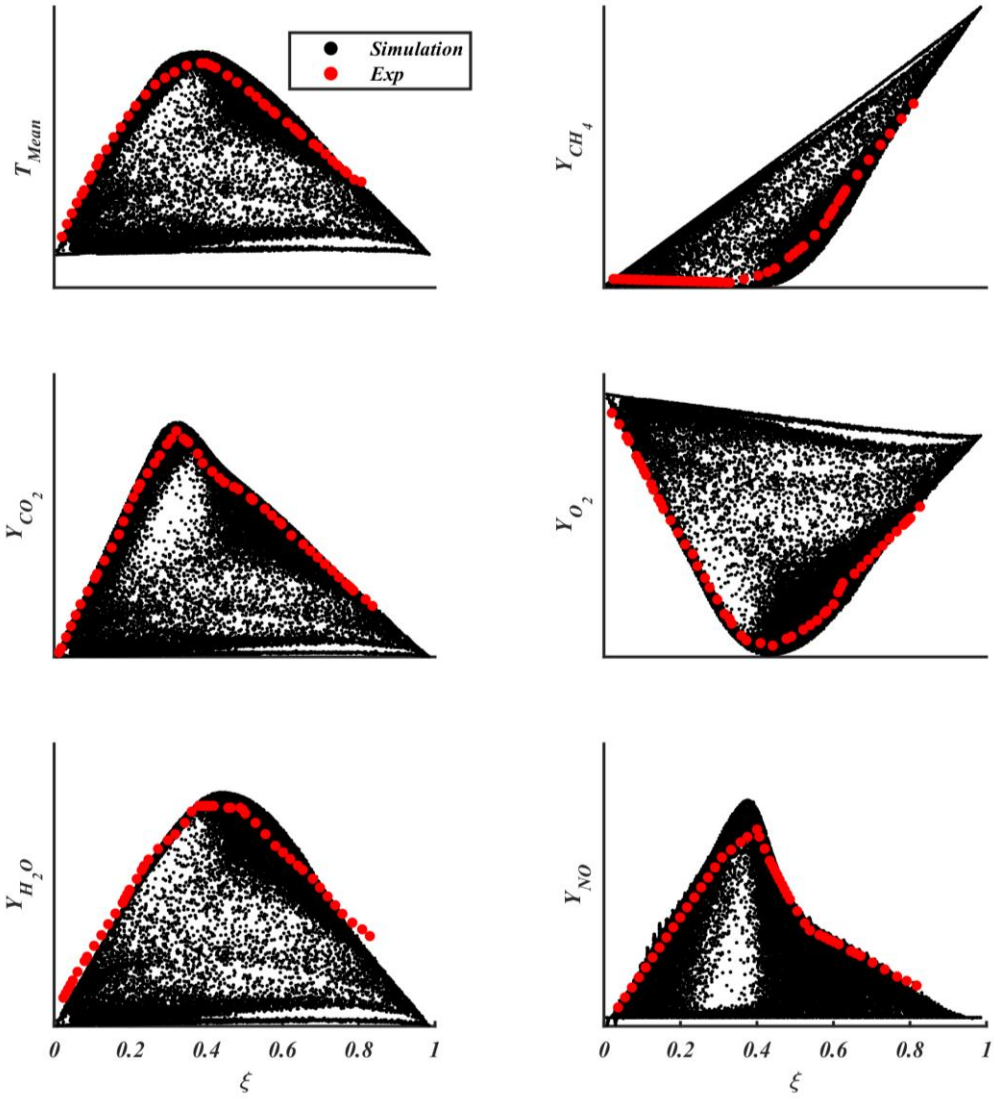

Figure 22: Scatter Plots for selected species at axial location of z/D =30 for MMC Model

A better comparison and validation for the simulations can be through conditional Averaged Values for scalar quantities presented against the mixture fraction (ξ) radially in Figure 23 and Figure 24. Three axial locations of $z/D = 15$, 30 and 45 are considered and will be discussed in the next go.

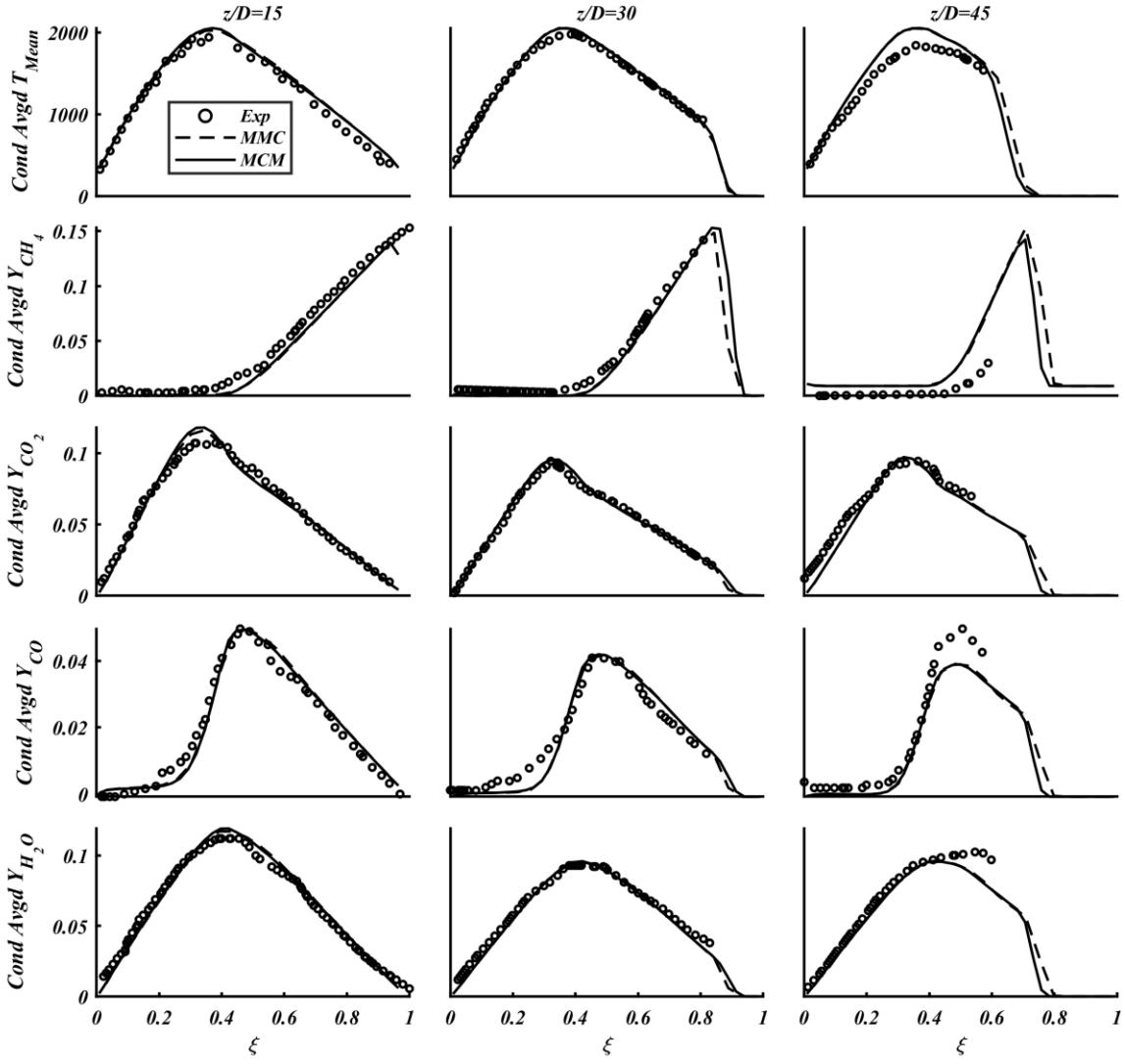

Figure 23: Conditional Statistics (1) for different axial locations in the computational domain

First at z/D =15, temperature and other species mass fraction seems to be in good agreement with the experimental results. Conversion of fuel to products is demonstrated by mass fractions of CO_2 and H_2O which are seen to be slightly overpredicted. Since mass fractions for O_2 and CH_4 are underpredicted, this can be very well the reason for the products overprediction. Temperature is also predicted good till a mixture fraction of $\xi = 0.6$ further with a small deviation from the branch. Moreover, a bump can be seen in cases of CO and H_2 which's been accurately predicted for CO whereas the latter having a 40 % increase from the experimental

value. Mass fraction for H_2 is generally overpredicted in many studies as well in the past [43-45]. Y_{OH} and Y_{NO} also show a sudden increase on the fuel lean side. Y_{NO} is seen to be quite overpredicted by a margin at a mixture fraction of $\xi = 0.5$ and goes improving gently towards the richer side. At z/D =30, temperature agrees with a good match up to mixture fraction of $\xi = 0.8$, further decreasing with a much faster rate than in the previous case. Prediction of mass fraction of main reactants (Y_{CH_4} & Y_{O_2}) and products (Y_{CO_2} & Y_{H_2O}) is in notable agreement with the experimental measurements. Improvements can also be noticed on the lean side of NO and OH, rich side of NO being notably underpredicted. Y_{H_2} which was overpredicted by a large extent in the previous case, shows satisfactory results in this case. Overall results can be considered to be very good in comparison to those of experimental ones. Variations are found negligible in most of the species.

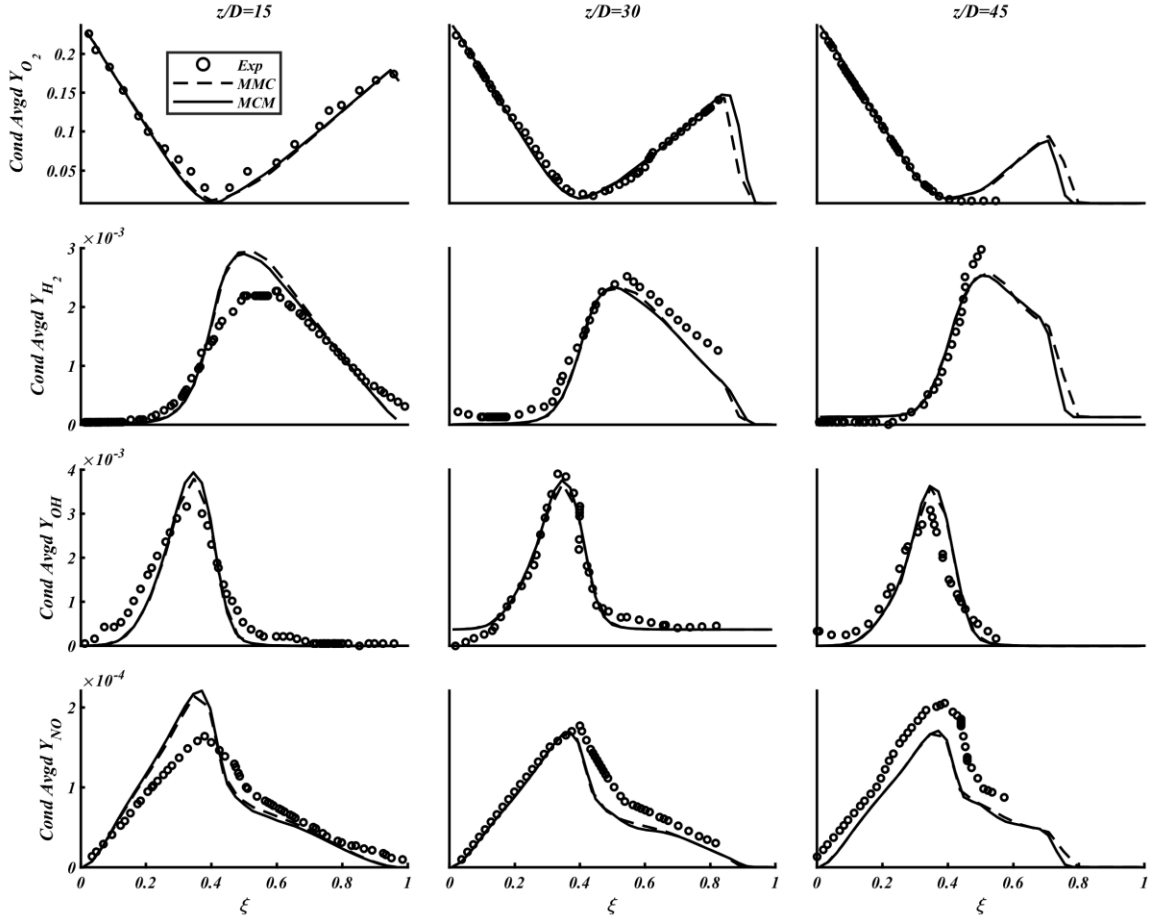

Figure 24: Conditional Statistics (2) for different axial locations in the computational domain

Finally, at z/D=45, since due to the lack of experimental data for some quantities at the rich side, simulation results are mainly validated against the data at the lean side and predictions have been stated. Temperature can be observed to be in good match on the lean side with a

sudden decrease after the mixture fraction of 0.6. Results for products i.e. Y_{CO_2} and Y_{H_2O} can be considered to be good on the lean side but Y_{H_2O} can be seen to be underpredicted. Out of reactants, Y_{O_2} seem to be in predicted good but Y_{CH_4} is overpredicted by a constant variation at least on the lean side. Similar constant deviation can be observed in Y_{NO} as well. Same plateau can be noticed for Y_{OH} and be considered in good agreement as in the previous locations.

8.2 Sydney Flame

Methodology proposed in section 7 about the partially premixed flames is carried out and time-averaged results for temperature and mass fractions for chemical species is presented in this section.

8.2.1 Validation

For validation of simulation results for Sydney flame, mean temperature at three axial locations (*z/D = 1,5 and 10*) are compared to the experimental results from [56] in Figure 25.

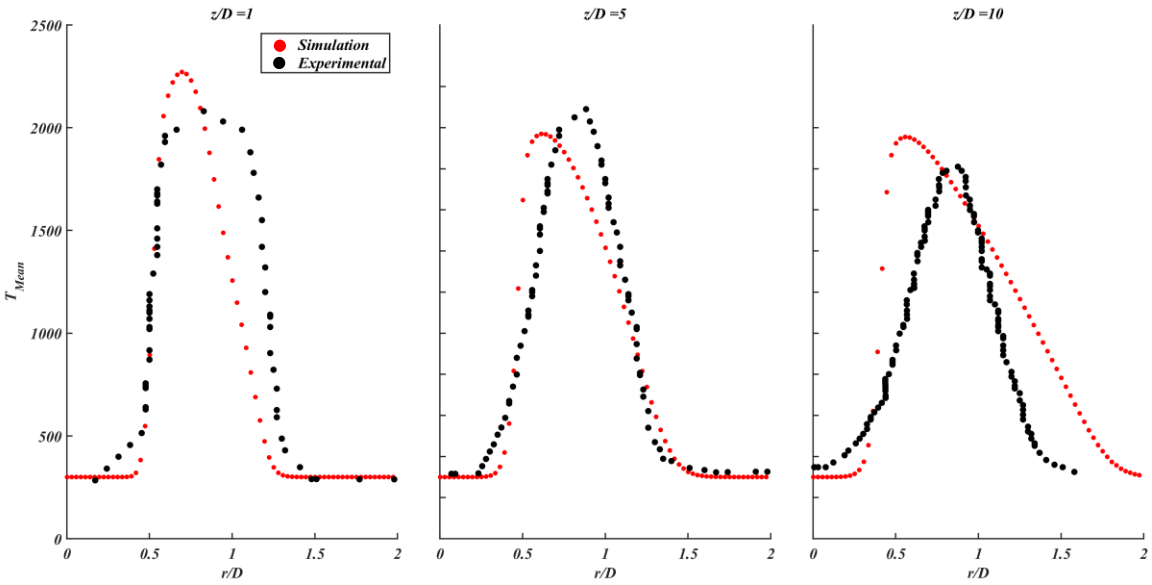

Figure 25: Time Averaged Temperature for three different axial locations

Since RANS is used for turbulence modelling with Finite Rate Chemistry in the aim to take Chemical Kinetics into account, an excellent agreement of simulation results with the experimental results can always definitely not be expected. However, in this case they are in the position that they can be validated to state further discussions. Temperature seems to be in good agreement at the starting (r/D = 0) and ending points (r/D >2) for all the three locations. Deviation of simulation results from experimental results in the positive slope region can be

observed to continuously increase in the axial direction, best being at the first one. Similar trend can be noticed in the plot with negative slope, with the best agreement in second one. Overall agreement can be considered to be as nominal for a study of behavior of other chemical species as discussed in case of Sandia Flame for this methodology as well.

8.2.2 General Results & Observations

In this sub-section, behavior of mass fraction for different chemical species CH_4, O_2, H_2O, CO_2 (Figure 26) and CO, H_2, OH, O_2 () will be discussed. Consequently, three axial locations z/D =1,5 and 10 have been considered. Unlike the previous cases, only simulation results will be presented followed by the validation in this section. 2D Contour plots for the same have also been presented along with the 2D plots.

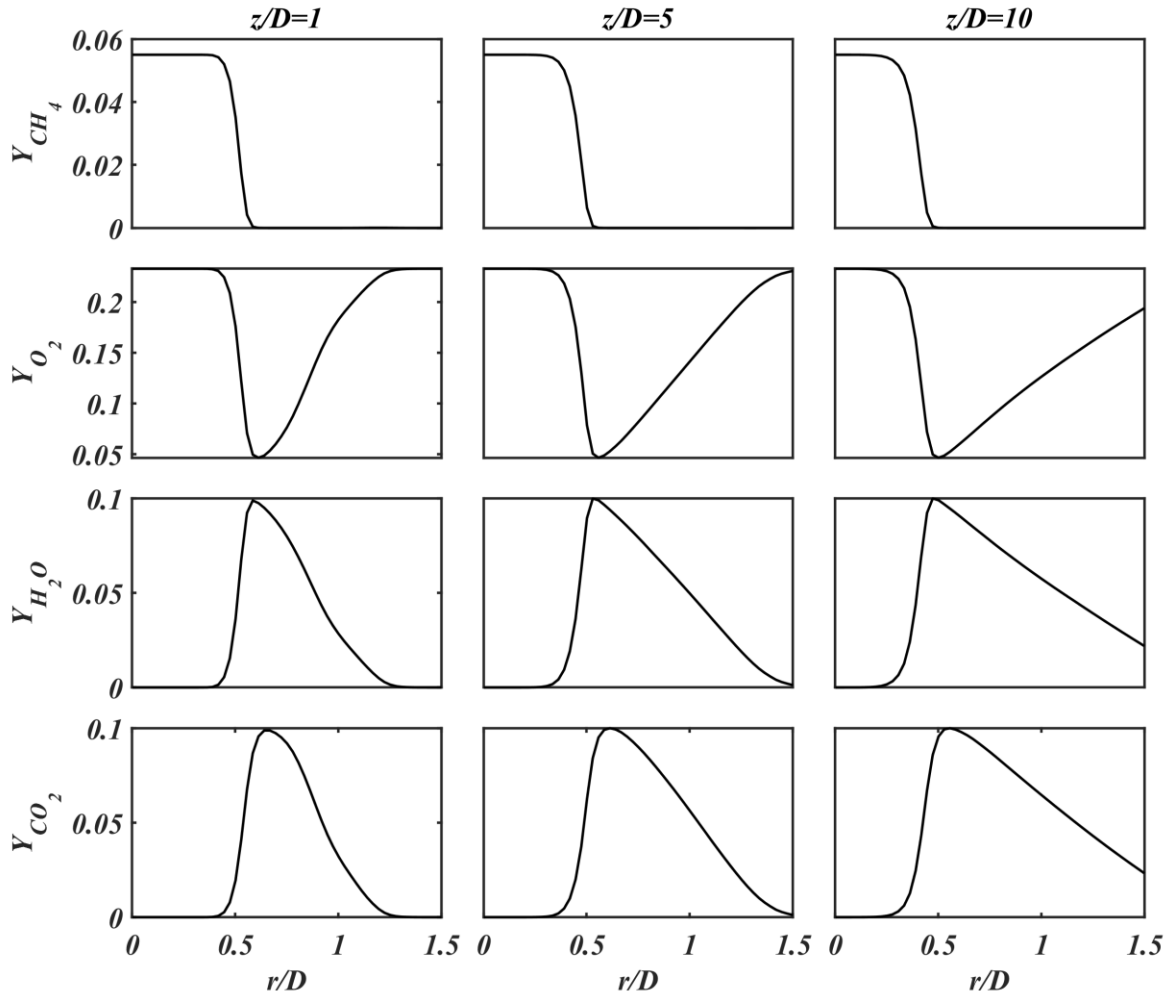

Figure 26: Mass fractions for mass fraction of chemical species CH_4, O_2, H_2O & CO_2 , at different axial locations

Firstly, the behavior of main products (CO_2 and H_2O) and reactants (CH_4 and O_2) is discussed. As observed in the Figure 26, mass fraction for methane and oxygen tend to stretch towards

the axial locations. Opposite behavior is seen from each other after r/D = 0.5. On the other hand, both the products show the similar trends.i.e. increasing a maximum value till r/D = 0.5 and further declining at a constant rate.

In the Figure 27, variations of mass fractions of chemical species CO, H_2, OH and N_2 over a particular radial section are shown. First three species, i.e. CO, H_2 and OH almost show a similar variation of increasing up to a certain limit and then decreasing logarithmically. N_2 can be expected to show a constant behavior till certain limit due to a limited availability in the air component.

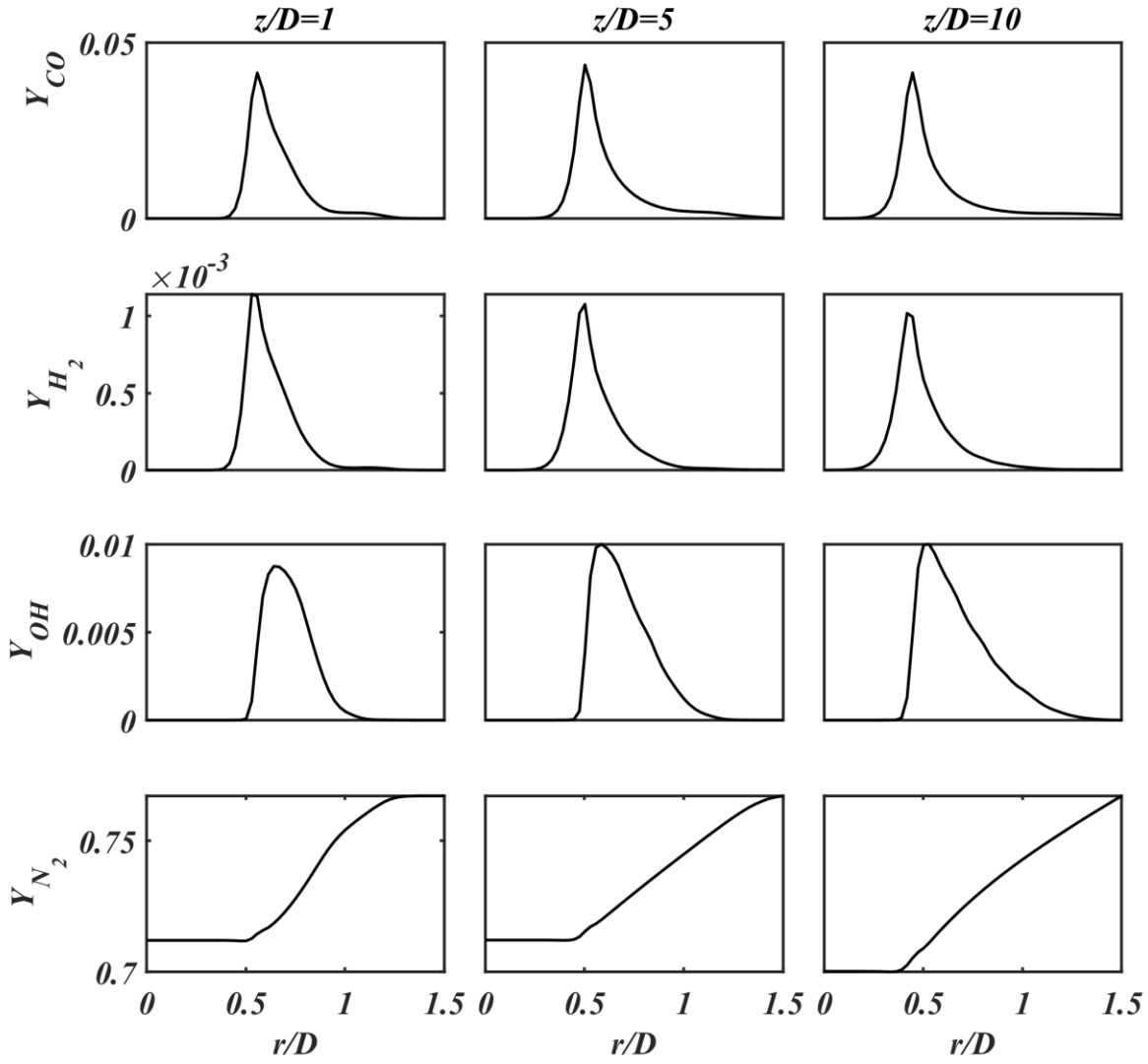

Figure 27: Mass fractions for mass fraction of chemical species CO, H_2, OH, N_2 at different axial locations

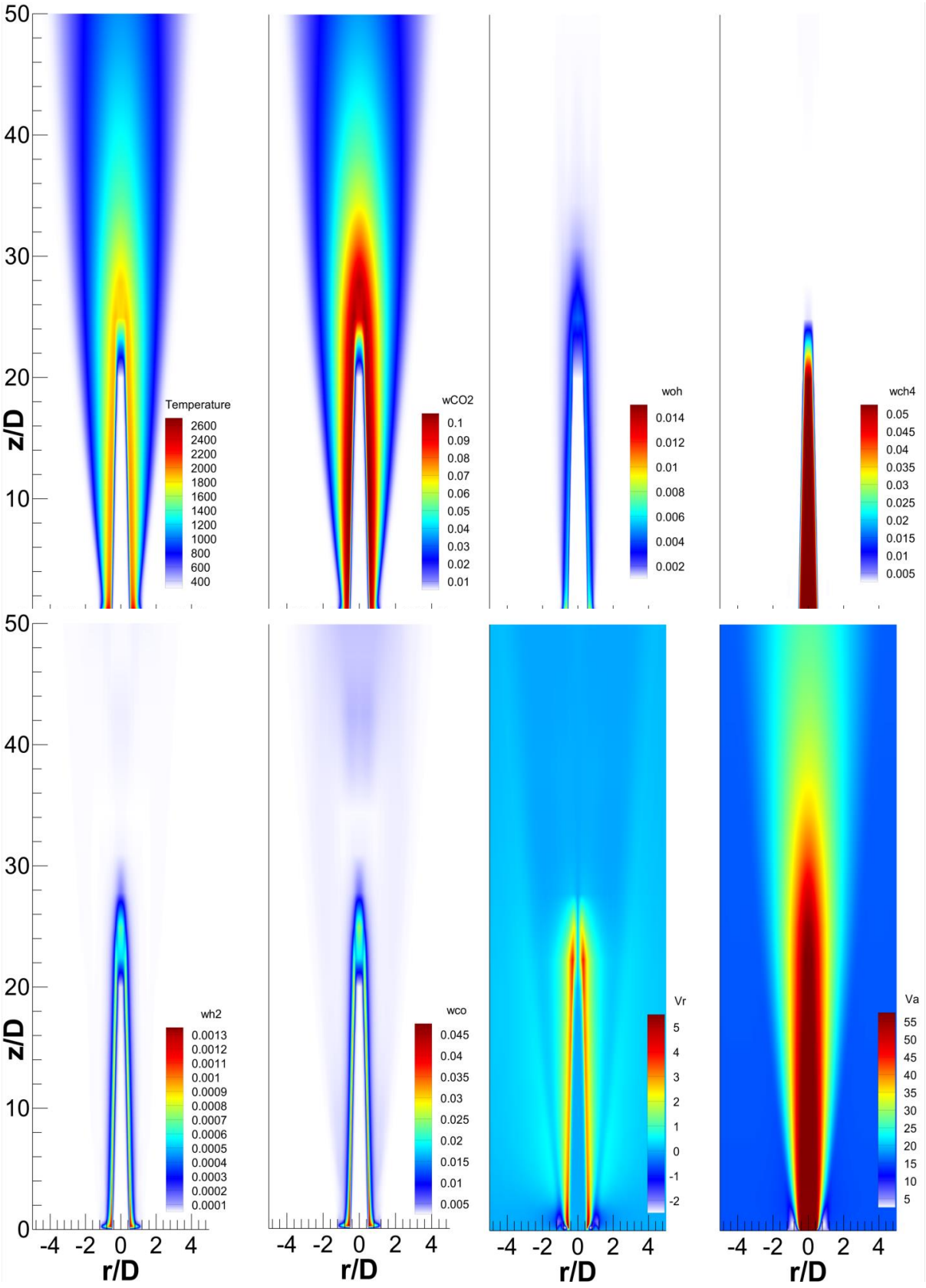

Figure 28: Contour Plots for major scalar quantities and Velocities (Axial and Radial)

9. Conclusion

9.1 Sandia Flame

Comparison of different time-averaged quantities along with their conditional averages variations for Sandia Flame D has been carried out using joint-composition PDF transport method for two different mixing models i.e. Modified Curl's Model and Velocity- Conditioned Multiple Mapping Closure. Both models have shown a good agreement of their predictions with the experimental data, each one of which is observed to satisfy criteria for choosing best value of number of particles needed for each CFD cell and the mixing parameter as described in section 8.1.

Since, MCM is found to be more computationally intensive than MMC, MMC can seem to be a good replacement for MCM model, former taking around 75,000 iterations as compared to latter with 3,50,000 - 4,00,000 to reach to a fully converged solution. Not only that, the best number of particles per cell found for each model are also less (20) in case of MMC in comparison with MCM (50). Overall, methodology for VC-MMC model is found to be quite good to be implemented or further development in combustion's research area especially in PDF composition transport model.

9.2 Sydney Flame

Sydney Flame has been successfully simulated in Ansys Fluent in order to get an overview of inhomogeneous mixing in partially premixed combustion. Standard $k - \epsilon$ turbulence model is used to take account of RANS with Finite Rate Chemistry (for Chemical Kinetics with GRI 3.0 Mechanism without NO_x and soot) with unity Lewis number assumption. It can be concluded that despite after a grid sensitivity test, Finite Rate chemistry is only able to well capture the turbulence chemistry interactions up to a certain limit. But for getting an overview and experience for such the piloted flames (which was the purpose of this work), this methodology has helped a lot to achieve the aim. Better methodology including approach to Large Eddy Simulations can be adopted to have better results.

References

[1] Williams, F.A. (1985). Combustion Theory: The Fundamental Theory of Chemically Reacting Flow Systems (2nd ed.). CRC Press. https://doi.org/10.1201/9780429494055

[2] Harles K. Westbrook, Frederick L. Dryer, Chemical kinetics and modeling of combustion processes, Symposium (International) on Combustion, Volume 18, Issue 1,1981, Pages 749-767, ISSN 0082-0784, https://doi.org/10.1016/S0082-0784(81)80079-3

[3] J. Warnatz, Ulrich Maas, Robert W. Dibble: Combustion: Physical and Chemical Fundamentals, Modelling and Simulation, Springer Science & Business Media, 2001 ISBN 9783540677512

[4] Echekki T., Mastorakos E. (eds) Turbulent Combustion Modelling. Fluid Mechanics and Its Applications, vol 95. Springer, Dordrecht. https://doi.org/10.1007/978-94-007-0412-1_2

[5] Santanu De, Avinash Kumar Agarwal, Swetaprovo Chaudhuri, Swarnendu Sen: Modeling and Simulation of Turbulent Combustion, Springer Singapore, 2018, ISBN 978-981-13-5628-5 https://doi.org/10.1007/978-981-10-7410-3

[6] John D. Anderson, Jr.: Fundamentals of Aerodynamics, McGraw-Hill Education, 2010, ISBN 9780073398105

[7] Pope, S. (2000). Turbulent Flows. Cambridge: Cambridge University Press. doi:10.1017/CBO9780511840531

[8] Yu, Chunkan. Numerical Simulation of Turbulent Flames based on Reaction-Diffusion Manifolds (REDIM) Reduced Chemistry,2020, Dissertation, Karlsruhe Institute of Technology (KIT) DOI: 10.5445/IR/1000124958

[9] Development and Validation of a Massively Parallel High-Order Solver for DNS and LES of Industrial Flows. In: Kroll N., Hirsch C., Bassi F., Johnston C., Hillewaert K. (eds) IDIHOM: Industrialization of High-Order Methods - A Top-Down Approach. Notes on Numerical Fluid Mechanics and Multidisciplinary Design, vol 128. Springer, Cham. https://doi.org/10.1007/978-3-319-12886-3_13

[10] Cant Stewart .2002 High-performance computing in computational fluid dynamics: progress and challenges Phil. Trans. R. Soc. A.3601211–1225 http://doi.org/10.1098/rsta.2002.0990

[11] A.R. Masri, Challenges for turbulent combustion, Proceedings of the Combustion Institute, Volume 38, Issue 1,2021, Pages 121-155, ISSN 1540-7489, https://doi.org/10.1016/j.proci.2020.07.144

[12] David Corson, Rajeev Jaiman & Farzin Shakib (2009) Industrial application of RANS modelling: capabilities and needs, International Journal of Computational Fluid Dynamics, 23:4, 337-347, DOI: 10.1080/10618560902776810

[13] Henk Kaarle Versteeg, Weeratunge Malalasekera: An Introduction to Computational Fluid Dynamics: The Finite Volume Method, Pearson Education, 2007, ISBN 9780131274983

[14] B.E. Launder, D.B. Spalding, The numerical computation of turbulent flows, Computer Methods in Applied Mechanics and Engineering, Volume 3, Issue 2,1974, Pages 269-289, ISSN 0045-7825, https://doi.org/10.1016/0045-7825(74)90029-2

[15] Henk Kaarle Versteeg, Weeratunge Malalasekera: An Introduction to Computational Fluid Dynamics: The Finite Volume Method, Pearson Education, 2007, ISBN 9780131274983

[16] S.B. Pope, PDF methods for turbulent reactive flows, Progress in Energy and Combustion Science, Volume 11, Issue 2,1985, Pages 119-192, ISSN 0360-1285, https://doi.org/10.1016/0360-1285(85)90002-4

[17] S. B. POPE (1981) A Monte Carlo Method for the PDF Equations of Turbulent Reactive Flow, Combustion Science and Technology, 25:5-6, 159-174, DOI: 10.1080/00102208108547500

[18] B.E. Launder, D.B. Spalding, The numerical computation of turbulent flows, Computer Methods in Applied Mechanics and Engineering, Volume 3, Issue 2,1974, Pages 269-289, ISSN 0045-7825, https://doi.org/10.1016/0045-7825(74)90029-2

[19] Renfeng Richard Cao, Haifeng Wang, Stephen B. Pope, The effect of mixing models in PDF calculations of piloted jet flames, Proceedings of the Combustion Institute, Volume 31, Issue 1,2007, Pages 1543-1550, ISSN 1540-7489, https://doi.org/10.1016/j.proci.2006.08.052

[20] César Dopazo, Edward E. O'Brien, An approach to the autoignition of a turbulent mixture, Acta Astronautica, Volume 1, Issues 9–10,1974, Pages 1239-1266, ISSN 0094-5765, https://doi.org/10.1016/0094-5765(74)90050-2

[21] R. L. Curl, Dispersed phase mixing: I. Theory and effects in simple reactors, Volume 9, Issue 2, 1963, Pages 175-181, https://doi.org/10.1002/aic.690090207

[22] Janicka, J., Kolbe, W. and Kollmann, W... "Closure of the Transport Equation for the Probability Density Function of Turbulent Scalar Fields", vol. 4, no. 1, 1979, pp. 47-66. https://doi.org/10.1515/jnet.1979.4.1.47

[23] S. B. POPE (1982) An Improved Turbulent Mixing Model, Combustion Science and Technology, 28:3-4, 131-145, DOI: 10.1080/00102208208952549

[24] P.A. Nooren, H.A. Wouters, T.W.J. Peeters, D. Roekaerts, U. Maas & D. Schmidt (1997) Monte Carlo PDF modelling of a turbulent natural-gas diffusion flame, Combustion Theory and Modelling, 1:1, 79-96, DOI: 10.1080/713665231

[25] Pope, S.B. Mapping closures for turbulent mixing and reaction. Theoret. Comput. Fluid Dynamics 2, 255–270 (1991). https://doi.org/10.1007/BF00271466

[26] Luis Valiño, Javier Ros, and César Dopazo, "Monte Carlo implementation and analytic solution of an inert-scalar turbulent-mixing test problem using a mapping closure", Physics of Fluids A: Fluid Dynamics 3, 2191-2198 (1991) https://doi.org/10.1063/1.857900

[27] Galindo Lopez, Sebastian, Modelling of Mixed-mode Combustion using Multiple Mapping Conditioning, 2018, Doctor of Philosophy Ph.D., University of Sydney; Faculty of Engineering and Information Technologies; School of Aerospace, Mechanical \& Mechatronic Engineering, http://hdl.handle.net/2123/19646

[28] Subramaniam, S. and S. Pope. "A mixing model for turbulent reactive flows based on Euclidean minimum spanning trees." Combustion and Flame 115 (1998): 487-514. https://doi.org/10.1016/S0010-2180(98)00023-6

[29] Cleary, M.J., Klimenko, A.Y. A Generalized Multiple Mapping Conditioning Approach for Turbulent Combustion. Flow Turbulence Combust **82,** 477 (2009). https://doi.org/10.1007/s10494-008-9161-3

[30] Carmen Straub, Santanu De, Andreas Kronenburg & Konstantina Vogiatzaki (2016) The effect of timescale variation in multiple mapping conditioning mixing of PDF calculations for Sandia Flame series D–F, Combustion Theory and Modelling, 20:5, 894-912, DOI: 10.1080/13647830.2016.1191677

[31] S. Galindo-Lopez, F. Salehi, M. Cleary, A. Masri, G. Neuber, O. Stein, A.Kronenburg, A. Varna, E. Hawkes, B. Sundaram, A. Klimenko, and Y.Ge, "A stochastic multiple mapping conditioning computational model in Open FOAM for turbulent combustion," Computers & Fluids, vol. 172, Pages 410 - 425, 2018.

[32] Stoellinger M., Efimov D., Roekaerts D. (2015) Monte Carlo Simulations of Turbulent Non-premixed Combustion using a Velocity Conditioned Mixing Model. In: Heinz S.,

Bessaih H. (eds) Stochastic Equations for Complex Systems. Mathematical Engineering. Springer, Cham. https://doi.org/10.1007/978-3-319-18206-3_7

[33] R. O. Fox, "On velocity-conditioned scalar mixing in homogeneous turbulence", Physics of Fluids 8, 2678-2691 (1996) https://doi.org/10.1063/1.869054

[34] A.Y. Klimenko,Matching conditional moments in PDF modelling of nonpremixed combustion,Combustion and Flame,Volume 143, Issue 4,2005,Pages 369-385,ISSN 0010-2180, https://doi.org/10.1016/j.combustflame.2005.08.014

[35] Andrew P. Wandel and A. Y. Klimenko,"Testing multiple mapping conditioning mixing for Monte Carlo probability density function simulations", Physics of Fluids 17, 128105 (2005) https://doi.org/10.1063/1.2147609

[36] Cleary M.J., Klimenko A.Y. (2011) Multiple Mapping Conditioning: A New Modelling Framework for Turbulent Combustion. In: Echekki T., Mastorakos E. (eds) Turbulent Combustion Modeling. Fluid Mechanics and Its Applications, vol 95. Springer, Dordrecht. https://doi.org/10.1007/978-94-007-0412-1_7

[37] R.S. Barlow, J.H. Frank, Effects of turbulence on species mass fractions in methane/air jet flames, Symposium (International) on Combustion, Volume 27, Issue 1,1998, Pages 1087-1095, ISSN 0082-0784, https://doi.org/10.1016/S0082-0784(98)80510-9

[38] Schneider, Ch & Dreizler, Andreas & Janicka, J. & Hassel, E... (2003). Flow field measurements of stable and locally extinguishing hydrocarbon-fuelled jet flames. Combustion and Flame - COMBUST FLAME. 135. 185-190. 10.1016/S0010-2180(03)00150-0

[39] Raman, Venkat & Pitsch, Heinz. (2007). A consistent LES/Filtered-density function formulation for the simulation of turbulent flames with detailed chemistry. Proceedings of the Combustion Institute. 31. 1711-1719. 10.1016/j.proci.2006.07.152

[40] Epaminondas Mastorakos, Ignition of turbulent non-premixed flames, Progress in Energy and Combustion Science, Volume 35, Issue 1,2009, Pages 57-97, ISSN 0360-1285, https://doi.org/10.1016/j.pecs.2008.07.002

[41] Giusti, A., Mastorakos, E. Turbulent Combustion Modelling and Experiments: Recent Trends and Developments. Flow Turbulence Combust 103, 847–869 (2019). https://doi.org/10.1007/s10494-019-00072-6

[42] De Bruyn Kops, S., Riley, J., Kosály, G. et al. Investigation of Modeling for Non-Premixed Turbulent Combustion. Flow, Turbulence and Combustion **60,** 105–122 (1998). https://doi.org/10.1023/A:1009986317078

[43] Large-eddy simulation of a turbulent piloted methane/air diffusion flame (Sandia flame D), Physics of Fluids 12, 2541-2554 (2000) https://doi.org/10.1063/1.128849

[44] Barlow, R S. Proceedings of the international workshop on measurement and computation of turbulent non-premixed flames. United States: N. p., 1996. Web. doi:10.2172/541794

[45] Cao, R.R. and Pope, S.B., "The influence of chemical mechanisms on PDF calculations of non-premixed piloted jet flames". In: Combustion and Flame, 143.4, 450-470, 2005 http://dx.doi.org/10.1016/j.combustflame.2005.08.018

[46] Steinhilber, G., Numerische Simulation turbulenter Verbrennungsprozessemittels statistischer Verfahren und REDIM reduzierter Kinetik. Dissertation. Karlsruhe, Karlsruhe Institut für Technologie (KIT), KIT Scientific Publishing, 2015

[47] Bykov, V.; Maas, U. Reduction of reacting flow models by the REDIM method, 21st ICDERS - July 23-27, 2007 – Poitiers DOI: 10.5445/IR/1000010856

[48] Jenny, P. and Pope, S. B. and Muradoglu, M. and Caughey, D. A., A Hybrid Algorithm for the Joint PDF Equation of Turbulent Reactive Flows, Journal of Computational Physics, Pages 218-252, 2001, https://doi.org/10.1006/jcph.2000.6646

[49] P. R. Van Slooten, Jayesh, and S. B. Pope, "Advances in PDF modelling for inhomogeneous turbulent flows", Physics of Fluids 10, 246-265 (1998) https://doi.org/10.1063/1.869564

[50] L.Y. Gicquel, G. Staffelbach, T. Poinsot, Large eddy simulations of gaseous flames in gas turbine combustion chambers, Prog. Energy Combust. Sci. 38(6) (2012) 782–817

[51] A. Tyliszczak, A. Bogusławski, D. Nowak, Numerical simulations of combustion process in a gas turbine with a single and multi-point fuel injection system, Appl. Energy 174 (2016) 153–165

[52] Lefebvre, A.H., & Ballal, D.R. (2010). Gas Turbine Combustion: Alternative Fuels and Emissions, Third Edition (3rd ed.). CRC Press. https://doi.org/10.1201/9781420086058

[53] M.C. Drake, D.C. Haworth, Advanced gasoline engine development using optical diagnostics and numerical modelling, Proc. Combust. Inst. 31(1) (2007) 99–124

[54] J.E. Dec, Advanced compression-ignition engines -understanding the in-cylinder processes, Proc. Combust. Inst. 32 ,2008, Pages 2727–2742.

[55] N. Syred, J.M. Beér, Combustion in swirling flows: A review, Combustion and Flame, Volume 23, Issue 2,1974, Pages 143-201, ISSN 0010-2180, https://doi.org/10.1016/0010-2180(74)90057-1

[56] R.S. Barlow, S. Meares, G. Magnotti, H. Cutcher, A.R. Masri, Local extinction and near-field structure in piloted turbulent CH4/air jet flames with inhomogeneous inlets, Combustion and Flame, Volume 162, Issue 10,2015,Pages 3516-3540,ISSN 0010-2180, https://doi.org/10.1016/j.combustflame.2015.06.009

[57] Prashant Shrotriya, Ping Wang, Linsong Jiang, Meenatchidevi Murugesan,REDIM-PFDF modelling of turbulent partially-premixed flame with inhomogeneous inlets using top-hat function for multi-stream mixing problem, Aerospace Science and Technology, Volume 107,2020,106258,ISSN 1270-9638, https://doi.org/10.1016/j.ast.2020.106258

[58] Hansinger, Maximilian & Zips, Julian & Pfitzner, Michael. (2019). Eulerian Stochastic Fields method and model free finite rate chemistry applied to Sydney partially premixed flame

[59] Tian, L and Lindstedt, RP, Transported PDF modelling and analysis of partially premixed flames, The Combustion Institute, 2017, http://hdl.handle.net/10044/1/48420

[60] Konstantin Kleinheinz, Thomas Kubis, Philipp Trisjono, Mathis Bode, Heinz Pitsch, Computational study of flame characteristics of a turbulent piloted jet burner with inhomogeneous inlets, Proceedings of the Combustion Institute, Volume 36, Issue 2,2017, Pages 1747-1757, ISSN 1540-7489, https://doi.org/10.1016/j.proci.2016.07.067

[61] Shaun Meares, Assaad R. Masri, A, Modified piloted burner for stabilizing turbulent flames of inhomogeneous mixtures, Combustion and Flame, Volume 161, Issue 2,2014, Pages 484-495, ISSN 0010-2180, https://doi.org/10.1016/j.combustflame.2013.09.016

[62] A. Lipatnikov, Stratified turbulent flames: recent advances in understanding the influence of mixture inhomogeneities on premixed combustion and modelling challenges, Prog. Energy Combust. Sci. 62 (2017) 1339–1351.

List of Figures

List of Tables